

Portland State University

PDXScholar

Environmental Science and Management
Faculty Publications and Presentations

Environmental Science and Management

7-1-2024

Modelling Postfire Recovery of Snow Albedo and Forest Structure to Understand Drivers of Decades of Reduced Snow Water Storage and Advanced Snowmelt Timing

A. Surunis

Portland State University

K. E. Gleason

Portland State University

Follow this and additional works at: https://pdxscholar.library.pdx.edu/esm_fac



Part of the [Environmental Studies Commons](#), and the [Physical and Environmental Geography Commons](#)

Let us know how access to this document benefits you.

Citation Details


Surunis, A., & Gleason, K. E. (2024). Modelling postfire recovery of snow albedo and forest structure to understand drivers of decades of reduced snow water storage and advanced snowmelt timing. *Hydrological Processes*, 38(7). Portico.

This Article is brought to you for free and open access. It has been accepted for inclusion in Environmental Science and Management Faculty Publications and Presentations by an authorized administrator of PDXScholar. Please contact us if we can make this document more accessible: pdxscholar@pdx.edu.

RESEARCH ARTICLE

WILEY

Modelling postfire recovery of snow albedo and forest structure to understand drivers of decades of reduced snow water storage and advanced snowmelt timing

A. Surunis  | K. E. Gleason

Department of Environmental Science and Management, Portland State University, Portland, Oregon, USA

Correspondence

A. Surunis, Department of Environmental Science and Management, Portland State University, Portland 97201, OR, USA.
Email: asurunis@pdx.edu

Funding information

NASA, Grant/Award Number: 80NSSC19K0002

Abstract

Forest fires darken snow albedo and degrade forest structure, ultimately reducing peak snow–water storage, and advancing snowmelt timing for up to 15 years following fire. To date, no volumetric estimates of watershed-scale postfire effects on snow–water storage and snowmelt timing have been quantified over decades of postfire recovery. Using postfire parameterizations in a spatially-distributed snow mass and energy balance model, SnowModel, we estimated postfire recovery of forest fire effects on snow–water equivalent (SWE) and snowmelt timing over decades following fire. Using this model, we quantified volumetric recovery of forest fire effects on snow hydrology across a chronosequence of eight sub-alpine forests burned between 2000 and 2019 in the Triple Divide of western Wyoming. We found that immediately following fire, forest fire effects reduced snow–water storage by 6.8% (SD = 11.2%) and advanced the snow disappearance date by 31 days (SD = 9 days). Across the 15-year recovery following fire, forest fire effects reduced snow–water storage by 4.5% (SD = 11.4%). Postfire effects on snow hydrology generally recovered over time, but still persisted beyond 15-years following fire due to the observed postfire shift from forest to open meadow. Estimates of postfire reductions on peak SWE summed over the entire 15-year postfire recovery period were 18 times greater than the immediate losses in the first winter following fire alone. These lasting effects of forest fires on snow hydrology decades following fire highlight the importance of postfire parameterizations for more accurate watershed-scale volumetric estimates of forest fire effects on snow–water resources.

KEYWORDS

forest fire, forest structure, modelling, snow, snow modelling, snow water equivalent, snowmelt, western US

This is an open access article under the terms of the [Creative Commons Attribution-NonCommercial-NoDerivs](https://creativecommons.org/licenses/by-nc-nd/4.0/) License, which permits use and distribution in any medium, provided the original work is properly cited, the use is non-commercial and no modifications or adaptations are made.

© 2024 The Author(s). *Hydrological Processes* published by John Wiley & Sons Ltd.

1 | INTRODUCTION

Climate warming threatens snow–water storage through feedbacks between declining snowpacks and increased forest fire activity (Fassnacht & López-Moreno, 2020; Gleason et al., 2019; Kampf et al., 2022; McGrath et al., 2023; Viviroli et al., 2007). The majority of water in the American West is seasonally stored in snowpack, with ecosystems and human communities relying on snowmelt as a source of water in the drier periods of late spring and summer (Li et al., 2017; Liu et al., 2022). Climate warming has reduced snow–water storage across the West, threatening downstream water availability (Alonso-González et al., 2022; Luce et al., 2013; Mote et al., 2018; Wieder et al., 2022). It is predicted that spring surface water availability will occur earlier, less reliably, and more episodically over the coming decades (Barnett et al., 2005; Hale et al., 2022; Wieder et al., 2022). Increasingly vulnerable snowpacks and associated earlier snowmelt have amplified forest fire activity across the West (Abatzoglou & Williams, 2016; Westerling, 2016), particularly in the densely forested seasonal snow zone where over 80% of western forest fires have burned since the 1980s (Gleason et al., 2013). Snow albedo, or the reflectivity of the snow surface, is a critical driver of the net snowpack shortwave radiation, which dominates the snowpack energy balance during spring snowmelt periods (Cline, 1997; Garvelmann et al., 2014; Marks & Dozier, 1992). Forest fire in the seasonal snow zone exacerbates the influence of warming climate on snowpacks through the postfire radiative forcing on snow, which includes the reduction of snow albedo due to the deposition of light absorbing particles onto snow and increased incoming solar radiation due to the degradation of forest trunks and forest canopy (Gleason et al., 2013, 2019; Gleason & Nolin, 2016; Smoot & Gleason, 2021). Here, we use the term “forest degradation” to define the progressive decline in aboveground forest structure that affects the snowpack energy balance (i.e., trunk and canopy) due to disturbance-induced mortality (delayed or otherwise) and direct structural damage.

Forest degradation and associated canopy removal by wildfire may enhance snow accumulation in winter through reduced canopy interception, but also influences snowpack energy balance and mass balance by increasing exposure to solar energy and wind-driven sublimation losses (Mooser et al., 2020; Ueyama et al., 2014). Forest degradation also reduces longwave radiative inputs to the snowpack from the surrounding forest canopy, particularly in warmer maritime snow climates (Lundquist et al., 2013). In continental regions where temperatures are colder and longwave radiative inputs from the forest canopy are small, additional shortwave radiative inputs from reductions in shading may outweigh the losses in longwave radiative inputs from forest structure degradation (Lundquist et al., 2013; Sicart et al., 2004). The overall net change in combined net shortwave and longwave radiative forcing on snowpack following canopy removal depends on the forest structure and snow climate (Lundquist et al., 2013; Musselman et al., 2008; Varhola et al., 2010). In addition to the enhanced radiation effects, forest canopy removal may also increase the turbulent fluxes at the snow surface ultimately reducing

snow–water storage and increasing snow melt rates (Harpold et al., 2014; McGrath et al., 2023).

Forest fires further alter the snowpack energy and mass balance due to the postfire radiative forcing on snow. Following forest fire, the more open forest canopy allows more incoming solar radiation incident on the snowpack surface, while the degradation of the post-fire forest canopy sheds black carbon and burned woody debris onto snowpack, which concentrates on the surface during snowmelt, darkening snow albedo and increasing the solar energy absorbed by the snowpack (Gleason et al., 2013, 2019; Gleason & Nolin, 2016). Increased radiative forcing on snow enhances the rate of snow metamorphism and the rate of snow albedo decay following fresh snowfall (Gleason et al., 2013; Gleason & Nolin, 2016). This postfire radiative forcing on snow profoundly increases the net snowpack shortwave radiation, which ultimately reduces peak snow water equivalent (SWE), and advances the timing of snowmelt and snow disappearance date (SDD) (Gleason et al., 2019; Smoot & Gleason, 2021; Stevens, 2017). Forest fire effects on snow hydrology including darker snow surface albedo, reduced snow–water storage, and earlier snowmelt extend across the burned forest area (Gleason & Nolin, 2016) and persist for at least 10 winters following fire across the West (Gleason et al., 2019; Smoot & Gleason, 2021). An interesting paradox is that at coarse spatial scales, postfire landscape-scale snow albedo brightened immediately following fire, and as the postfire forest degraded over time and revealed more of the snowpack beneath burned forests resembled an open meadow after 15 years following fire (Gersh et al., 2022).

High-severity burned forests are composed of dead and dying trees that fall apart in the years following fire (Dunn & Bailey, 2012) exposing greater snow surface areas to solar radiative forcing (Gersh et al., 2022). Postfire forest degradation and subsequent regeneration of high-elevation evergreen forests often spans decades to centuries depending on fire severity, fire extent, distance to seed sources, elevation, and climate such as postfire drought conditions (Busby et al., 2020; Coop et al., 2010; Dunn & Bailey, 2012; Vanderhoof et al., 2021; Viana-Soto et al., 2022). In some cases, such as high-elevation dry and moist forests occurring at the edge of their climatic tolerance, forests do not regenerate back to prefire conditions and instead convert to non-forests especially towards the interior of the burned area (Harvey et al., 2016; Rodman et al., 2020; Stevens-Rumann et al., 2018; Stevens-Rumann & Morgan, 2019). Combined with postfire radiative forcing on snow, delayed postfire forest regeneration or forest-to-open conversion in the seasonal zone, may sustain postfire forest structural changes and associated shifts in snow–water storage for decades following fire.

To date, no study has quantified volumetric estimates of postfire effects on snow–water storage and snowmelt timing across burned forested areas and over the decades of postfire recovery. Forest fires are extensive and increasing in occurrence across the West, changing forest structure and ultimately snow hydrology over vast regions (Burles & Boon, 2011; Dennison et al., 2014; Westerling, 2016) that are difficult to quantify through in situ measurements alone. The limited spatial extent of in situ measurements and coarse resolution of

satellite-based remote sensing observations make process-based snow evolution models a critical tool enabling spatially distributed volumetric estimates of postfire effects on snow–water storage and snowmelt timing over decades following fire.

In order to understand the recovery of postfire effects on snow hydrology and, by extension, water resource availability, we used a physically-based spatially-distributed snow mass and energy balance model, with best estimate postfire parameterizations to estimate volumetric forest fire effects on snow–water storage and snowmelt timing over decades following fire. We focused on a chronosequence of eight forests, burned from 2000 to 2019, in the Triple Divide region of western Wyoming to answer the research question: what is the modelled magnitude and persistence of postfire volumetric effects on snow–water storage (SWE) and snowmelt timing (SDD) over the snow season and over years since fire? Our primary goal is to provide the most informed estimates of the magnitude of postfire volumetric changes to snow hydrology, based on the best available data, parameterizations, and modelling. We aim to provide best guess estimates of the magnitude of postfire volumetric changes to snow hydrology to help to guide decision-making and improve streamflow forecasting of water resource managers over decades of postfire recovery. As climate warms and snowpacks are ever more vulnerable, while forest fires increase in occurrence and extent across the West, estimates of postfire effects on snow albedo, forest structure, and ultimately snow hydrology over decades following fire are vital for future land management and water resource planning.

2 | MATERIALS AND METHODS

Our approach to evaluate recovery of changes in snow hydrology due to postfire effects on snow albedo and forest structure relied on best estimate parameterizations employed in a physically-based spatially-distributed snow evolution model. Across a chronosequence of eight burned forests, burned from 2000 to 2019, we compared modelled snow volume outputs between an unparameterized base model, a postfire forest structure model, and a combined postfire forest structure and postfire snow albedo model, in forest fire perimeters and at the watershed scale. All climatic variables were held constant between models allowing us to compartmentalize and directly compute postfire effects on snow storage and snowmelt. We evaluated impacts to snowpack energy and mass balance from postfire forest structure degradation and postfire snow albedo reductions seasonally, immediately following fire, and over decades following fire. We also compared modelled results with limited field observations of SWE collected in the chronosequence of burned forests by a field team during February and March of 2019 and 2020.

2.1 | Study region

We modelled and evaluated the postfire recovery on snow hydrology across a chronosequence of eight forests burned from 2000 to 2019

in the seasonal snow zone of the Triple Divide region in western Wyoming (Figure 1). The modelled domain of our study region was determined by calculating a minimum bounding rectangle around the chronosequence of burn perimeters taken from the Monitoring Trends in Burn Severity (MTBS) burn perimeters dataset (Finco et al., 2012) plus a 2 km buffer (Figure 1). The study area has an average elevation of 2503 m with a minimum and maximum elevation of 1727 m and 3596 m (Danielson & Gesch, 2011). Between 2000 and 2019, the average cold season (December to March) air temperature was -7.7°C ($\text{SD} = 5.5^{\circ}\text{C}$), and the region received an average annual precipitation of 110 cm (NOAA, 2021; Saha et al., 2011; USDA-NRCS, 2020; Western Regional Climate Center, 2021). The study region is largely forested, consisting of 60% forested land and 40% unforested land (35% shrub, grassland, and agricultural, 0.006% urban, and 4% bare rock) based on Copernicus Global Landcover data (Buchhorn et al., 2020). The forested land is pine-dominated, of which the most common species are Lodgepole Pine (*Pinus contorta*) and Whitebark Pine (*Pinus albicaulis*). Our study region covers the Triple Divide region of three major river basins of the western US, including the Colorado, Columbia, and Missouri Rivers. This area has a history of frequent forest fire and has experienced a rapid increase in the extent, severity, duration, and occurrence of forest fire in the seasonal snow zone over recent decades (Frankson et al., 2022). The Triple Divide region is an ideal test bed for investigations into our primary research question and for better understanding the magnitude and persistence of postfire effects on snow hydrology. This understanding is critical to preserving snow–water resource availability in this region and for understanding postfire effects on snow–water storage and snowmelt broadly across the West.

2.2 | SnowModel description

To estimate the recovery of forest fire effects on snow–water storage and snowmelt across burned forests over decades following fire, we used a physically-based spatially-distributed snow evolution model called SnowModel. SnowModel is a process-based model that uses first-order physics to simulate snow accumulation, blowing-snow redistribution and sublimation, snow-density evolution, and snowpack melt over spatially varying topography and landcover grids driven by temporally varying meteorological forcing fields (Liston et al., 2007; Liston & Elder, 2006a, 2006b). SnowModel was used in this study because of its foundation in first-order physics, ready customizability, and extensive validation in forested, montane seasonal snowpack similar to our study region (Hiemstra et al., 2006; Liston et al., 2007; Liston & Elder, 2006a, 2006b; Sextone et al., 2018).

SnowModel utilizes four sub-models in a hierarchal modelling structure including MicroMet, EnBal, SnowPack-Multilayer (SnowPack-ML), and SnowTran-3D. MicroMet spatially interpolates meteorological forcing data from meteorological stations observations and/or modelled reanalysis meteorological outputs of air temperature, precipitation, wind speed, wind direction, air pressure, and relative humidity (Liston & Elder, 2006a). Using a spatially weighted Barne's

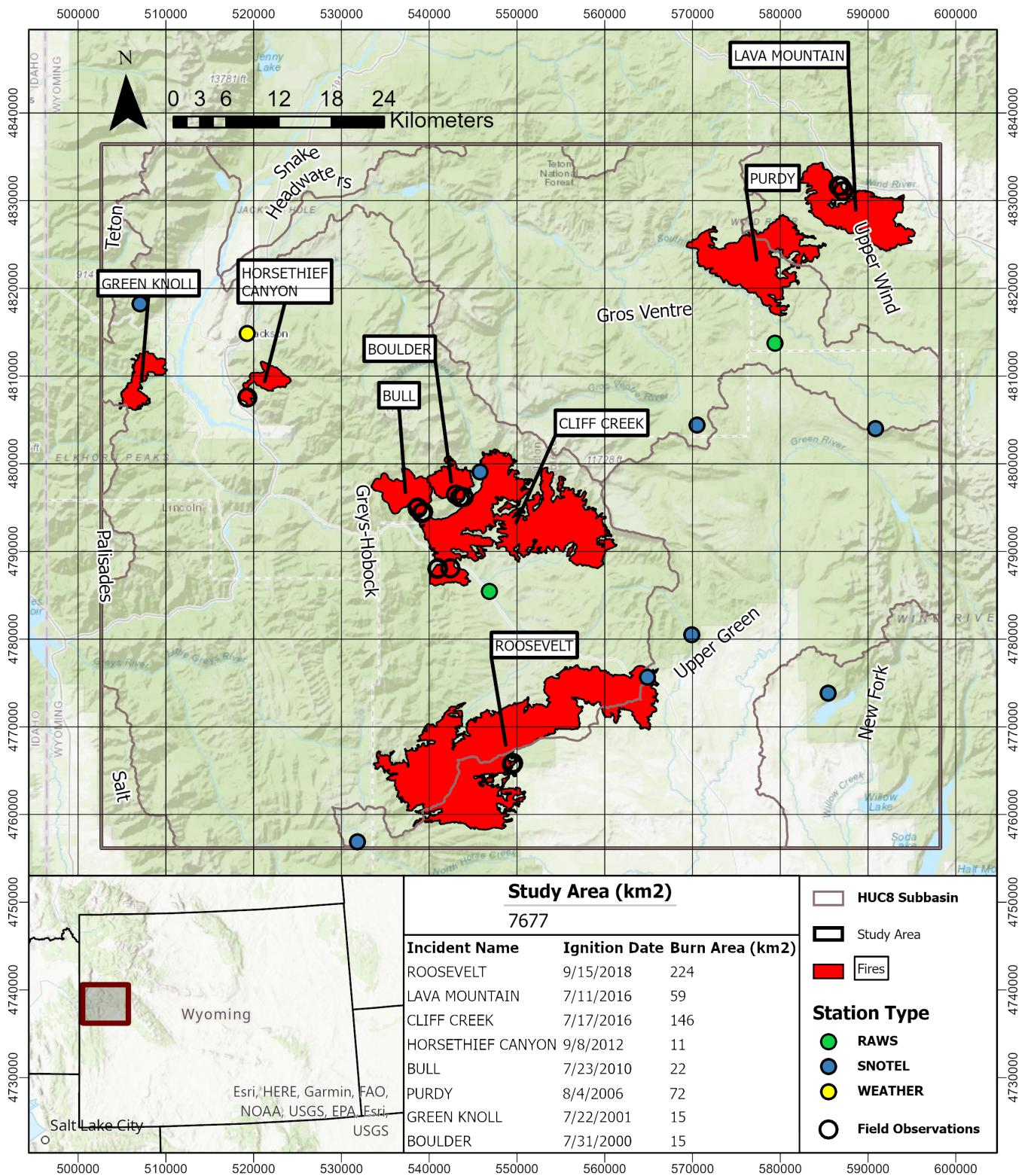


FIGURE 1 A map of the study region and modelling domain. The map includes Monitoring Trends in Burn Severity fire boundaries of the eight fires that occurred in the study region over the modelling time period along with their ignition date, incident type, and total burn area. The location and type of meteorological stations that the in situ meteorological forcing data was drawn from are shown and the boundaries of the HUC-8 sub-basins and their names are also displayed.

interpolation method, MicroMet produces a meteorological forcing field for every cell in the simulation for every time step (Liston & Elder, 2006b). MicroMet also estimates incoming shortwave and

longwave radiation inputs in each cell using solar calculations based on the latitude of the study region and parametrizations of cloudiness (Liston & Elder, 2006a). EnBal utilizes the outputs of MicroMet and

physics-based mass energy balance equations to calculate the snow mass and energy balance of the snowpack within every cell at every time step of the simulation and, critical to our application, is where modelling of forest-snow interactions are handled (Liston & Hall, 1995). SnowTran-3D is a three-dimensional model that incorporates the wind-flowing forcing field from MicroMet and topographical and vegetation inputs to compute redistribution of snow due to wind and loss of snow by saltation and wind-induced sublimation (Liston et al., 2007). SnowPack-ML computes snow-density through temperature- and compaction-based snow-density evolution (Liston & Elder, 2006b). SnowPack-ML can be run using a single layer or up to 12 distinct layers and simulates cold content, permeability, and liquid water release from the snowpack within each cell for every time step (Liston & Elder, 2006b).

We made modifications to SnowModel, which parameterize postfire snow albedo decay and postfire forest canopy degradation and their recovery over time. Using outputs from this parameterized model, we generated informed volumetric estimates of postfire effects on snow hydrology and the evolution of these effects over postfire recovery. A brief overview of how SnowModel models snow accumulation and snowmelt follows, however a full description of SnowModel operations for snow albedo and snowpack in forests can be found in Liston and Elder (2006a). To simulate forest-snow interactions, SnowModel uses several sub-models to simulate canopy interception, canopy loading and unloading, sublimation of intercepted snow, and radiation transmission through forest canopies. SnowModel incorporates several forest canopy metrics within these calculations including effective leaf area index, canopy height, snow-holding depth, gap fraction, and forest type. Each of these variables plays a role in determining snow-depth evolution at each time step of the model and the resulting SWE in each cell. To simulate snow albedo, the default SnowModel-EnBal assigns a constant snow albedo value to each cell depending on landcover type (forested, non-forested, or glacier ice) and accumulating or melting snowpack.

2.2.1 | SnowModel parameterizations

We incorporated parameterizations of key postfire effects on snow hydrology including, postfire snow albedo and postfire forest structure over years following fire, to estimate the immediate and persistent volumetric changes and recovery of snow-water storage and timing of snowmelt following fire. Our postfire snow albedo decay and recovery model utilized the postfire snow albedo decay parameterization from Gleason and Nolin (2016) and a postfire forest structure degradation parameterization informed by long-term trends in MODIS-derived landscape snow albedo from Gersh et al. (2022). Gleason and Nolin (2016) derived empirical snow albedo decay functions from broadband snow albedo measurements taken in adjacent burned and unburned forested sites over 3 years following fire in the high-elevation lodgepole pine forests of the Oregon Cascades. These snow albedo exponential decay functions reduce snow albedo over

days since fresh snowfall differentially for burned and unburned forested sites and open meadows and for cold and warm snow periods throughout the snow season (Gleason & Nolin, 2016). The postfire snow albedo recovery trends over 15 years following fire were informed by Gersh et al. (2022), who characterized postfire snow albedo recovery over years following fire in a chronosequence of eight burned forests in the Triple Divide region of Wyoming burned between 2000 and 2019, the same burned forests modelled in this study. Gersh et al. (2022) utilized MODIS-MOD10A1 estimates of landscape-scale snow albedo and determined that postfire landscape snow albedo more resembled that of open areas than antecedent pre-fire forest conditions after 15 years following fire. Other studies have also indicated that high-elevation burned forests, typical of our study region in the Rocky Mountains, experience slow or delayed postfire regeneration over two to three decades (Coop et al., 2010; Vanderhoof et al., 2021), which can be delayed further by the occurrence of postfire drought (Viana-Soto et al., 2022). In many other studies, high-elevation coniferous burned forests similar to our study region, did not regenerate back to prefire forest conditions at all and instead converted to grass or shrubland (Harvey et al., 2016; Stevens-Rumann et al., 2018; Stevens-Rumann & Morgan, 2019). Postfire forest structure conversion to open land cover was also observed in field visits to the eight forest fires modelled in this study (Figure 2). We acknowledge that forest regeneration continues beyond 15 years following fire, and that our postfire parameterizations of forest structure represent a snapshot of postfire recovery up to two decades following fire in high-elevation burned forests such as the Triple Divide region of western Wyoming.

2.3 | SnowModel input data retrieval

SnowModel requires a minimum of three primary inputs including meteorological forcing data, a topographic elevation raster, and a landcover classification raster. Meteorological forcing data were retrieved from both automated weather stations and modelled reanalysis data. In situ meteorological forcing data from automated weather stations were retrieved from the United States Department of Agriculture (USDA) National Resources Conservation Service (NRCS) automated Snow Telemetry (SNOTEL) network (USDA-NRCS, 2020) from the National Weather and Climate Center (NWCC) data retrieval tool (<https://wcc.sc.egov.usda.gov/reportGenerator>). SNOTEL data were supplemented with additional in-situ weather data from the Western Regional Climate Center (WRCS) Remote Automated Weather Station (RAWS) network (Western Regional Climate Center, 2021), and the National Oceanic and Atmospheric Administration (NOAA) Climate Data Online (CDO) network (NOAA, 2021) to capture a wider range of weather variability over an elevation range (Table S1). Hourly measurements of air temperature, precipitation, wind speed, wind direction, and relative humidity were retrieved from each of these stations, and daily average values of each were calculated over the entire modelling period (WY2000-WY2020) for use in SnowModel. In addition, daily SWE values were retrieved from the

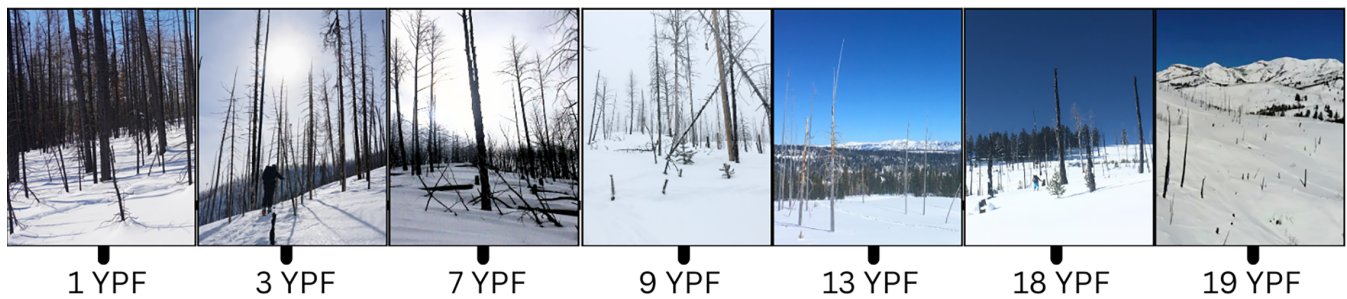


FIGURE 2 Field site photos of burned forests taken on-site in April 2019 show forest structure transitioning to open land cover as a function of years postfire (YPF). Forest fires and ignition years listed left to right: Roosevelt (2019), Cliff Creek (2016), Horsethief Canyon (2012), Bull (2010), Purdy (2006), Green Knoll (2001), and Boulder (2000).

nine SNOTEL stations in our model domain for SWE assimilation and calibration of SnowModel.

The in situ meteorological data were supplemented with data from Climate Forecast System version 2 (CFSv2) modelled reanalysis meteorological data from the NOAA National Centers for Environmental Prediction (NCEP) (Saha et al., 2011). CFSv2 pixels were converted into “virtual” weather stations using R’s (R Core Team, 2021) “spatial” package (v7.3–12; Venables & Ripley, 2002), where the coordinates of each “station” were taken as the centroid of the pixel and elevation was taken as a product of geopotential height at the surface. This process effectively produced an ordered grid of weather stations with micrometeorological forcing data across the model domain. Daily values of temperature, precipitation, wind speed, and wind direction were averaged from 6-hourly values, and relative humidity was computed using daily averaged specific humidity value, daily average temperature, and the Clausius-Clapeyron relation (O. L. I. Brown, 1951).

Digital elevation maps (DEMs) and landcover classifications were retrieved using Google Earth Engine, a cloud-based GIS platform (Gorelick et al., 2017). A DEM of the region was retrieved from the Global Multi-resolution Terrain Elevation Dataset (GMTED) 2010 (Danielson & Gesch, 2011). GMTED is a product of the NASA Shuttle Radar Topography Mission (SRTM), which generated a DEM of elevation data at a resolution of 1 arc-second. Landcover data was retrieved from the Copernicus Global Land Cover 2015–2019 dataset, which classifies 23 different classes of landcover at a 100 m resolution (Buchhorn et al., 2021). Landcover data was reclassified to match the land classes defined by SnowModel. Both raster layers were clipped to the model domain, used at their native resolutions of 100 m, and converted to ASCII using R’s (R Core Team, 2021) “spatial” package (v7.3–12; Venables & Ripley, 2002).

2.4 | SnowModel calibration

SnowModel was calibrated by running the base model (i.e., a model with no burn parameters or burn classes applied) iteratively using varying sets of parameter values for gap fraction, snowfall fraction calculations, number of snowpack layers and snowpack layer width, and scalars applied to air temperature and precipitation forcing data. Following each run, modelled SWE values were compared to the time-

series of observed SWE values from the SNOTEL stations in the study region. For calibration purposes, four of the nine SNOTEL stations were excluded from the meteorological inputs to be used as calibration-only stations. The landcover class of individual grid cells containing SNOTEL stations was set to open meadow to reflect the forest clearings where SNOTEL stations were located. Modelled values of SWE at the observation locations were extracted by locating the cell containing each SNOTEL station and compared to the associated observed SWE measured by the SNOTEL station for that time step. Modelled versus observed SWE was plotted over all 20 years of the simulation (Figure S3). Performance metrics were then calculated between modelled SWE and the observed SNOTEL SWE measurements using root-squared error (RSE), Nash-Sutcliffe Efficiency (NSE), R-squared (R^2), and percent bias (PBIAS) (Moriassi et al., 2007). Pixel values were extracted using the “spatial” package (v7.3–12; Venables & Ripley, 2002) within R (R Core Team, 2021) and the performance statistics were calculated using the “HydroGOF” package (v0.4–0; Mauricio Zambrano-Bigiarini, 2020). Optimized parameter sets were found that met the performance thresholds outlined by Moriassi et al. (2007) following 21 calibration runs (Table S2; Figure S3). The best calibration was found using the default parameters of SnowModel, but with the modelled (CFSv2) precipitation inputs increased by 18.5%, an amount consistent with previous research from Yuan et al. (2011) that found that CFSv2 modelled reanalysis data can underestimate precipitation results by up to 20%. The precipitation scalar was optimized by running the model with progressively increasing scalar values until the performance thresholds were met. We avoided tuning this value further to avoid overfitting our model. After calibration, SnowModel overestimated SWE by 11.40% across all stations, a level of overestimation acceptable given the performance thresholds determined by Moriassi et al. (2007) ($|PBIAS| < 15\%$) (Table S2). All subsequent model runs maintained consistent parameter values to evaluate the influence of postfire model parameterizations outside the individual calibrated model parameters.

2.5 | Model descriptions

We utilized three model structures to estimate how postfire effects on snow albedo and forest structure degradation altered snowpack

volume and snowmelt timing over the decades of postfire recovery including, the base model, a postfire forest structure recovery model, and a combined postfire snow albedo and forest structure recovery model. By differencing the modelled results of the postfire forest model or postfire forest and snow model, from the base model, while holding all meteorological forcing data constant, we isolated and estimated the postfire effects of snow albedo and/or postfire forest degradation on snow–water storage volume and snowmelt timing across burned forests and over decades following fire.

2.5.1 | Base model

The base model used the default calibrated SnowModel parameters to compare against the results of the postfire snow albedo and postfire forest structure recovery models. This model accounted for no postfire effects on snow albedo or forest structure and effectively represents a “no-burn” scenario within the study region. The base model included a forest and open meadow snow albedo decay parameterizations derived from Gleason and Nolin (2016), but no postfire parameterizations.

2.5.2 | Postfire forest structure recovery model

The postfire forest structure model consisted of the calibrated base model described above, with the addition of time-varying postfire forest structure recovery parameterizations that simulated the postfire forest structure degradation over 15 years following fire to an open meadow. No postfire effects on snow albedo were included in the postfire forest structure recovery model. The postfire forest structure recovery model allowed for isolation of postfire effects on snow hydrology due solely to forest structure changes following fire.

2.5.3 | Postfire snow albedo recovery model

The postfire snow albedo recovery model consisted of the calibrated base model described in 2.5.1, plus the forest structure recovery parameterizations described in 2.5.2, as well as postfire snow albedo parameterizations from Gleason and Nolin (2016) recovering over 15 years following fire. This model simulated the postfire effects on snow albedo, and forest structure and recovered these parameters to that of an open meadow over the course of 15 years following fire.

2.5.4 | Recovery of postfire snow albedo and forest structure parameterizations

To represent the recovery of postfire snow albedo and forest structure parameterizations over 15 years following fire, our parameterizations included five unique snow albedo and forest structure recovery stages each representing 3 years of recovery (Figure 3). The 3-year

postfire recovery staged the snow albedo functions and forest structure parameters applied to each burned forest, by assigning custom burned forest classes to grid cells in the burn perimeters over 15 years following fire. These stages utilized five sets of snow albedo minimum, snow albedo maximum, snow albedo decay functions, and forest structure parameters, calculated by equally spacing snow albedo and forest structure parameters between the immediate postfire forest condition and an open meadow after 15 years following fire. Immediate postfire forest conditions for snow albedo minimum, maximum, and decay curves for burned forests, unburned forests, and open meadows were drawn from Gleason and Nolin (2016). Forest structure was parameterized by modifying the snow-holding depth (SHD) of burned forest cells over the five unique recovery stages from the date of forest fire ignition to beyond 15 years following fire. The SHD value is used in SnowModel to calculate the snow holding capacity of vegetation within each grid cell. The snow depth of a cell must exceed the SHD value before snow can reach the ground and become affected by wind redistribution, wind ablation effects, and canopy-modified solar forcing all of which ultimately modify the resulting SWE of the grid cell. For more information, SHD and supporting literature are explained in detail by (Liston & Elder, 2006a).

The postfire snow albedo parameterization solved for daily mean snow albedo using a time-varying exponential decay coefficient, where the minimum and maximum snow albedo values and the snow albedo decay function were modified to recover across the five unique periods over 15 years following fire. The snow albedo decay parameterization reset snow albedo values following a fresh snowfall event (>5 cm), and then exponentially decayed over days following fresh snowfall using recovery stage specific coefficients. Maximum snow albedo ($\alpha_{\text{snow,max}}$) represented the snow albedo of fresh snowfall in burned forests, unburned forests, and open meadows as defined by Gleason and Nolin (2016). Maximum snow albedo postfire recovery ($\Delta\alpha_{\text{snow,max}}$) was calculated as the difference between maximum snow albedo $\alpha_{\text{snow,max}}$ and the snow albedo of fresh snowfall in an open meadow divided by five (the number of three-year recovery periods in 15 years of postfire recovery). The fresh snowfall recovery rate was scaled by the number of 3-year recovery periods since forest fire (p) and added to $\alpha_{\text{snow,max}}$ to produce the snow albedo of fresh snowfall in a burned forest during recovery (Equation 1).

$$\alpha_{\text{snow}} = \alpha_{\text{snow,max}} + (p * \Delta\alpha_{\text{snow,max}}) \quad (1)$$

In burned forests, snow albedo decayed using an exponential decay coefficient that was adjusted to account for postfire recovery periods over 15 years following forest fire (Equation 2). Snow albedo in days-following-snowfall ($\alpha_{\text{snow}}^{n+1}$) was calculated as defined in Gleason and Nolin (2016) and Equation 1 except the minimum snow albedo of a burned forest ($\alpha_{\text{snow,min}}$) and the exponential snow albedo decay rate (K_a) were adjusted by the minimum snow albedo recovery rate ($\Delta\alpha_{\text{snow,min}}$) and the snow albedo decay recovery rate (ΔK_a), respectively, with each rate scaled by the current recovery period (p).

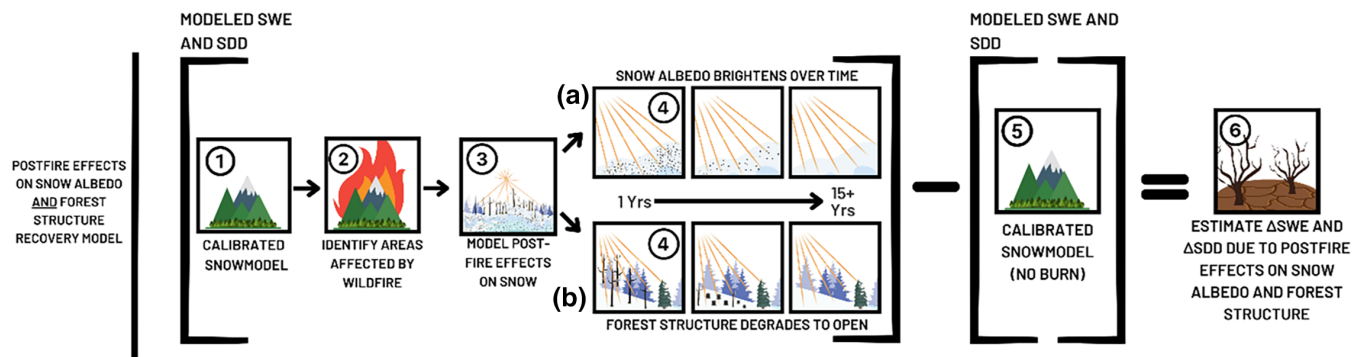


FIGURE 3 A conceptual model of the postfire effects on (a) snow albedo and (b) forest structure recovery model. SnowModel was first calibrated to the study region (1) to produce a base, unparameterized “no-burn” model. Areas affected by forest fires were identified (2). Postfire effects on snow albedo and/or forest structure were parameterized within SnowModel (3) and recovered over time (4) to produce models A and B. The SWE and SDD results from models A and B were differenced from the “no-burn” model (5) to compute estimates of postfire effects on snow due to forest structure degradation and/or snow albedo darkening (6).

$$(\alpha_{\text{snow}})^{n+1} = (\alpha_{\text{snow, min}} + \Delta\alpha_{\text{snow, min}} * p) + \left((\alpha_{\text{snow}})^n - (\alpha_{\text{snow, min}} + \Delta\alpha_{\text{snow, min}} * p) \right)^{\left[\frac{(-K_a + \Delta K_a * p) * dt}{1} \right]}$$

To simulate the postfire forest structure “recovery” of landcover change from burned forest to an open meadow, the custom burned forest class snow-holding depths start at a SHD value of 8.00 (roughly half that of an unburned coniferous forest) immediately following fire and progressed to a SHD value of an open meadow (0.25) in five 3-year steps over 15 years following fire (Equation 3).

$$SHD_{\text{burn}} = SHD_{\text{forest}} - (\Delta SHD * p) \quad (3)$$

The snow-holding depth of the burned forest (SHD_{burn}) was equal to the starting snow-holding depth value (SHD_{forest}) adjusted by the forest structure recovery rate (ΔSHD) scaled by the number of three-year recovery period since the forest fire occurred (e.g., 1–3 years postfire: $p = 0$, 4–6 years postfire: $p = 1$, etc.).

2.6 | Analysis of model results

2.6.1 | Postfire effects on snow–water storage and snow disappearance date timing

Postfire effects on snow hydrology were estimated by differencing modelled results of SWE and SDD from the default base model, and the parameterized postfire forest structure recovery model and the postfire forest structure and snow albedo recovery model. Forest fire effects on snow–water storage were evaluated by differencing postfire peak SWE rasters from base model peak SWE rasters for each year in the 20-year modelling period (2000–2020). Peak SWE rasters were created by determining the maximum SWE for each grid cell across the domain for each water year. Postfire peak SWE rasters were differenced from the base model peak SWE rasters, then

averaged across each burned forest in the chronosequence for each 3-year period during the 15-year recovery following fire. Volumetric changes in peak SWE for each burned forest were calculated by multiplying the peak SWE differences by the spatial resolution (100 m²), summing the volumetric differences of each grid cell within each burn region, and then averaging the total volumetric change in peak SWE across the 3-year recovery period. Postfire effects on snow disappearance date were quantified by determining the day-of-year of snow disappearance, for each grid cell, for each water year, and differencing the postfire snow albedo or forest structure model SDD from the base model SDD value. SDD was defined as the first day following peak SWE in which a grid cell reached below 5 mm SWE for each year. Differences in SDD were then averaged over the first year postfire, each three-year period following fire, and all years beyond 15 years (16+) following the fire ignition date.

2.6.2 | Recovery of postfire effects on snow hydrology

Postfire effects on snow–water equivalent were evaluated within each burn perimeter both seasonally and annually across all years available in the modelling period following fire. Seasonal changes in SWE were evaluated by differencing SWE outputs between the base model and the parameterized postfire models on March 1st (generally representing accumulation), April 1st (generally representing start of ablation), and May 1st (generally representing ablation). The differenced March 1st, April 1st, and May 1st SWE rasters were then averaged for each 3-year periods across the 15-year postfire recovery period. The average proportional change in SWE and 95% confidence interval were also calculated for each raster. Daily SWE niveographs were created for each burned forest for each 3-year recovery period to highlight differences in snow accumulation and ablation in recovering burned forests across the entire snow season. Each point on the daily SWE niveographs were computed by averaging all SWE values within the burn perimeters over each day and then each three-year

recovery period (Figure S3). All calculations were computed using base R (R Core Team, 2021) and the “spatial” package (v7.3–12; Venables & Ripley, 2002).

2.6.3 | Recovery of watershed-scale postfire effects on snow hydrology

Aggregated watershed-scale postfire effects and recovery on ablation season (May 1st) SWE were investigated within the Lower Granite Creek Hydrologic Unit Code 12 (HUC12) subbasin. Three of the eight burned forests from the chronosequence included in the modelling domain (Boulder, Bull, and Roosevelt) occurred entirely or partially within the Lower Granite Creek (LGC) subbasin between 2000 and 2020. The Boulder Fire burned in 2000 and burned entirely within the LGC subbasin (Boulder Fire burned 15 km², 13.05% of the watershed area), the Bull and Cliff Creek Fires burned partially within the LGC subbasin in 2010 and 2016 (Bull fire burned 12 km², 10.48% of the basin; and Cliff Creek Fire burned 23 km², 19.81% of the basin. In combination, all three fires burned 50.45 km² or 43.37% of the total watershed area over the 20-year modelling period. We focused on the ablation season for two reasons: (1) postfire effects on snow hydrology were most pronounced following peak SWE, and (2) estimations of SWE reductions due to postfire effects would likely be most applicable to watershed managers during the snowmelt season when snowpack is transitioning to surface water inputs. A United States Geological Survey (USGS) delineation of the watershed was extracted using the Living Atlas tool in ArcGIS (Esri Inc., 2022) and exported into R (U.S. Geological Survey National Geospatial Program, 2022). Annual postfire changes in ablation season SWE were estimated by calculating the average proportional and volumetric differences in SWE across the watershed between the base model and parameterized postfire snow albedo and forest structure model. Total postfire SWE change over the 20-year modelling period was calculated by summing the differences in May 1st SWE between the base model and postfire forest structure and snow albedo recovery model and converting to volume by area of the watershed. Annual ablation season (May 1st) SWE rasters were similarly derived by differencing the base model SWE rasters and postfire forest structure and snow albedo recovery model SWE rasters across the watershed, and plotted using the “spatial” package (v7.3–12; Venables & Ripley, 2002) in R (R Core Team, 2021).

2.6.4 | Statistical analysis

We tested for differences between the base model and postfire snow albedo and forest structure recovery models using the extracted values of annual peak SWE, annual SDD, seasonal SWE (March 1st, April 1st, and May 1st), and ablation season watershed-scale SWE (May 1st). Differences between the base model and postfire snow albedo and forest structure recovery model results were tested using a two-sided, two-sample Welch *t*-test using an alpha value of 0.05. All

results were analysed using a subset of paired random samples from 20% of the grid cells within each burn region from the base model and postfire snow albedo and forest structure recovery model rasters and running the statistical analysis using base functions in R (R Core Team, 2021).

2.6.5 | Model evaluation

Modelled SWE outputs from the base model and postfire snow albedo and forest structure recovery models were evaluated using in-situ field measurements of SWE taken from six of the modelled burned forests (Horsethief Canyon, Bull, Boulder, Cliff Creek, Lava Mountain, and Roosevelt) during February and March of 2019 (Figure 1). At each high or moderate severity measurement site within the burn perimeters, one to three replicates of SWE measurements were taken but, due to the close proximity of the replicates and the modelling resolution of 100 m², replicates were averaged as typically fell within the same modelled grid cell. Average measured SWE values were then matched with corresponding modelled SWE results from the base model and postfire snow albedo and forest structure recovery model, and the average percentage difference was computed between the observed and modelled values. An overall average percent difference was calculated by computing average percentage difference between all observed measurements and the associated base model SWE and postfire snow albedo and forest structure recovery model SWE. Observed vs modelled SWE comparisons were constrained due to the limitations of the situ measurements, which were limited in temporal and spatial extent, as they were a snapshot in time and not of adequate spatial scale for statistical evaluation.

3 | RESULTS

3.1 | Summary

Model results demonstrated that parameterizations of postfire reductions in snow albedo and forest structure degradation decreased snow–water storage (SWE) and advanced snow disappearance date persistently for at least 15 years following fire (Table 1). Immediately following fire, snowpack volume increased slightly during the accumulation period (March 1st) but increased solar forcing from postfire canopy loss and postfire reductions in snow albedo drove earlier melt onset, leading to substantial reductions during the ablation period (April 1st and May 1st) snowpack volume (Figure 4; Table S3b,c). Earlier melt onset resulted in reduced peak SWE and earlier SDD immediately following fire and altered snowpack energy balance, which persisted throughout the 15-year postfire recovery period (Figures 5 and 6) with the greatest reductions in peak SWE occurring 1 to 3 and 7 to 9 years following fire (Table 1). Burned forests modelled after the 15-year postfire recovery period still showed lasting changes in peak SWE and SDD 16+ years following fire (Figure 5; Table 1). At the watershed-scale, postfire effects and recovery of three burns

TABLE 1 Differences in snow water equivalent (SWE) (<1-year postfire, per 3-year period, and total) and differences in snow disappearance date (SDD) between the base model and postfire snow albedo and forest structure recovery model. Nearly all modelled fires showed reductions in peak SWE and advances in SDD relative to the base model in every recovery period following fire. Cells are coloured in severity of the change for each burn, with red indicating more severe losses and blue indicating relative gains. The ignition year, total burn area, average elevation, and altitudinal variability for each burn region are included above. Asterisks are also shown on all SWE metrics denoting the level of significant difference between the base model and postfire snow albedo and forest structure recovery model (* $p < 0.05$, ** $0.001 < p < 0.01$; *** $p < 0.0001$).

Burn	Immediate peak SWE loss (<1 YPF)	Period 1 (1–3 YPF)	Period 2 (4–6 YPF)	Period 3 (7–9 YPF)	Period 4 (10–12 YPF)	Period 5 (13–15 YPF)	Post-rec. (16+ YPF)	Total peak SWE change (1–15 YPF)
Boulder	-7.87%***	-7.6%***/ 4.0%	-5.3%***/ 3.0%	-5.4%***/ 3.5%	-1.1%***/ 7.1%	-2.7%*/ 2.7%	+1.9%***/ 3.2%	-4.1%***
Green Knoll	-16.93%***	-11.9%***/ 4.1%	-14.9%***/ 4.4%	-7.1%***/ 8.3%	-6.7%***/ 3.9%	-6.0%***/ 5.5%	-2.5%***/ 4.1%	-8.1%***
Purdy	-6.28%***	-3.5%***/ 9.7%	+0.3%***/ 11.5%	-2.0%***/ 6.3%	+1.0%***/ 5.2%	+4.5%***/ 7.8%		-0.7%
Bull	-1.43%	-9.2%***/ 5.7%	-6.0%***/ 1.9%	-7.0%***/ 3.4%	-0.1%/ 6.3%			-6.3%***
Horsethief Canyon	-23.65%***	-14.9%***/ 4.7%	-11.0%*/ 5.3%	-6.3%*/ 2.8%				-10.6%***
Lava Mountain	-7.50%***	-6.1%***/ 3.7%	+5.3%*/ 9.2%					-3.6%***
Cliff Creek	-9.11%***	-7.0%*/ 6.4%	-4.3%*/ 11.1%					-6.1%***
Roosevelt	-9.34%***	-6.9%***/ 7.5%						-6.5%***
Avg. Peak SWE Change (%)	8.4%***/ 9.4%	-6.8%***/ 11.2%	-3.1%***/ 13.4%	-3.9%***/ 8.7%	-0.9%/ 9.4%	+0.9%/ 9.8%	-0.3%/ 4.3%	-4.5%***/ 11.4%
Avg. Peak SWE Change (m ³)	5.0 M	-8.1 M***/ 7.5 M	-1.8 M***/ 1.8 M	-2.3 M***/ 1.2 M	-0.2 M/ 1.3 M	+0.6 M/ 3.0 M	-0.1 M/ 0.3 M	-11.0 M***/ 7.0 M
Avg. Peak SWE Change (mm)	67.8 M	-44.2***/ 72.6	-20.4***/ 80.8	-28.7***/ 56.1	-2.0/ 57.2	+8.2/ 55.3	-5.8/ 33.1	
Avg. SDD Shift (days)	-34 days***/ 7 days	-31 days***/ 9 days	-27 days***/ 13 days	-22 days***/ 8 days	-17 days***/ 6 days	-8 days***/ 6 days	-5 days***/ 6 days	

Note: The grey shade is present to indicate that there is no data for forest fires at the given date range.

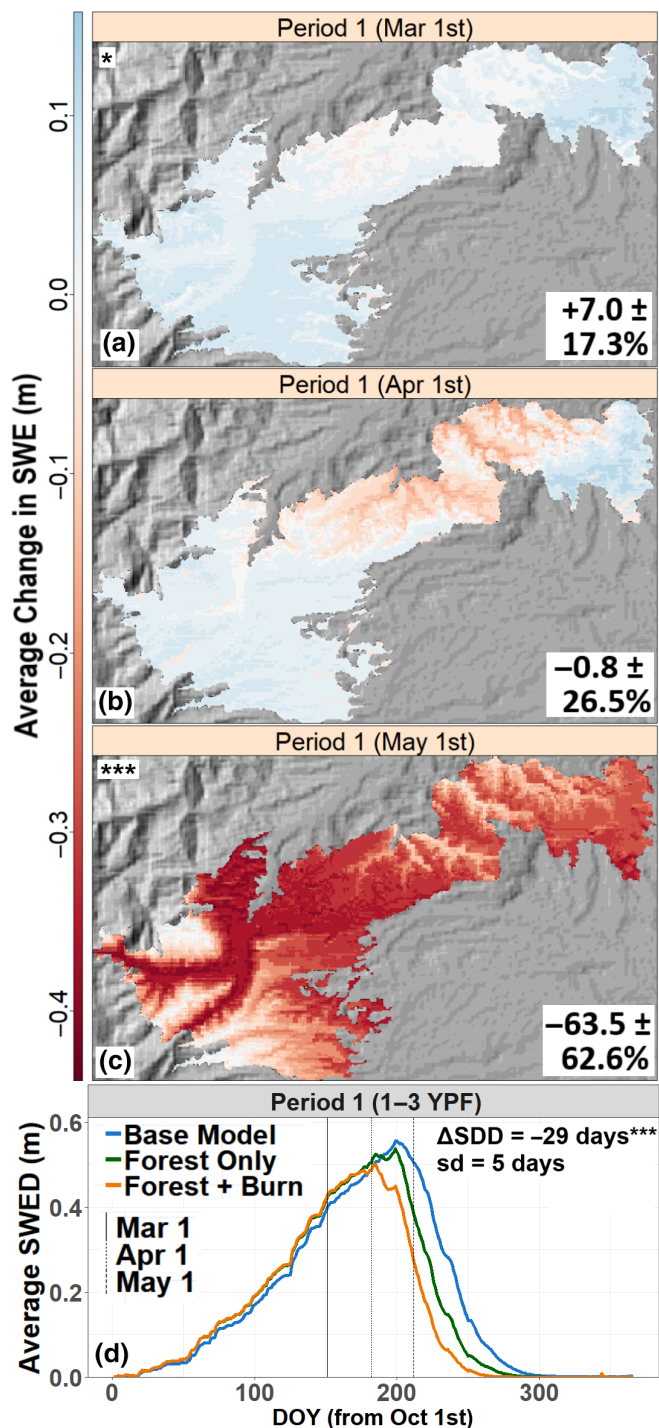


FIGURE 4 Change in snow–water equivalent (SWE) depth between the base model and postfire snow albedo recovery model in Roosevelt Forest Fire (Ignition Year: 2018). Postfire effects caused small increases in average March 1st SWE (a), no significant difference in average April 1st SWE (b), and large reductions in average May 1st SWE (c) across the burn region. Prior to April 1st, the average SWE of the postfire forest and postfire albedo model was greater than the base model (d).

modelled in the Lower Granite Creek subbasin reduced ablation season SWE (May 1st) in all but 1 year, with the greatest net reductions in ablation season SWE occurring 3–5 years following fire (Figure 7).

Even with variability between individual fires, there was a consistent overall pattern of immediate and lasting postfire effects and recovery on SWE and SDD, which we describe in detail using two burned forests as examples including, the Roosevelt fire, burned in 2019, and the Green Knoll Fire burned in 2001.

3.2 | Immediate postfire effects on snow volume and snow disappearance date

In the first winter immediately following fire, modelled postfire effects on snow albedo and forest structure decreased peak SWE by over 8% (peak SWE $\mu = -8.42\%$, $\sigma = 9.38\%$; $p < 0.001$; Table 1) and advanced SDD by 5 weeks (SDD $\mu = -34$ days, $\sigma = 7$ days; $p < 0.001$; Table 1) across all burned forests. Immediately following fire, peak SWE reductions varied across individual burned forests (1-year range of -1.43% to -23.65% , 1–3 year range of -3.52% to -14.85% ; Table 1), likely due to heterogeneity in prefire landcover, postfire burn severity, and topography and relative associated snowpack energy balance. In the first few years (1–3 years) following fire, SDD advanced by over a month across all modelled burned forests (SDD $\mu = -31$ days, $\sigma = 9$ days; $p < 0.001$; Table 1). During the accumulation period (March 1st) peak SWE increased ($\mu = +5\%$, $\sigma = 8\%$; $p < .001$; Table S3a), during historical peak SWE (April 1st) peak SWE decreased ($\mu = -5.8\%$, $\sigma = 16.2\%$; $p < 0.001$; Table S3b), and during the ablation period, peak SWE decreased substantially ($\mu = -51.6\%$, $\sigma = 33.6\%$; $p < 0.001$; Table S3c) across all eight modelled burned forests.

As an example of immediate postfire effects on snow–water storage and snowmelt timing, we focus on one large recent modelled forest fire, The Roosevelt Fire, which burned in 2019. Changes in peak SWE in the Roosevelt Fire were consistent with the broader changes observed across all modelled forest fire immediately following fire (peak SWE $\mu = -9.34\%$; $p < 0.001$; Table 1). Over the first two winters following the Roosevelt Fire included in the modelling extent (2019 and 2020), accumulation season SWE (March 1st) increased ($\mu = +7.0\%$, $\sigma = 8.6\%$, $p = 0.017$; Table S3a) due to the more open postfire forest canopy structure. The postfire forest structure model and postfire snow albedo and forest structure recovery models showed nearly identical increases in average SWE during March (Figure 4d). While the postfire snow albedo and forest structure model demonstrated reductions in SWE later in the snow season as a result of the net increase in shortwave radiation in spring (Figure 6a). Average April 1st SWE in the postfire snow albedo and forest structure recovery model did not differ from the base model, likely because the increase in March 1st SWE observed earlier was offset due to earlier melt onset from postfire effects on snow albedo (Figure 4d) and resulting increase in snowpack net shortwave radiation on snowpack (Figure 6a). After April 1st, melt onset began in earnest in the postfire snow albedo and forest structure recovery model, while snow continued to accumulate until mid to late April in the base model and postfire forest structure recovery model (Figure 4d). This indicated that earlier melt onset was primarily due to postfire effects on snow albedo and associated net shortwave radiation. By the ablation season (May 1st),

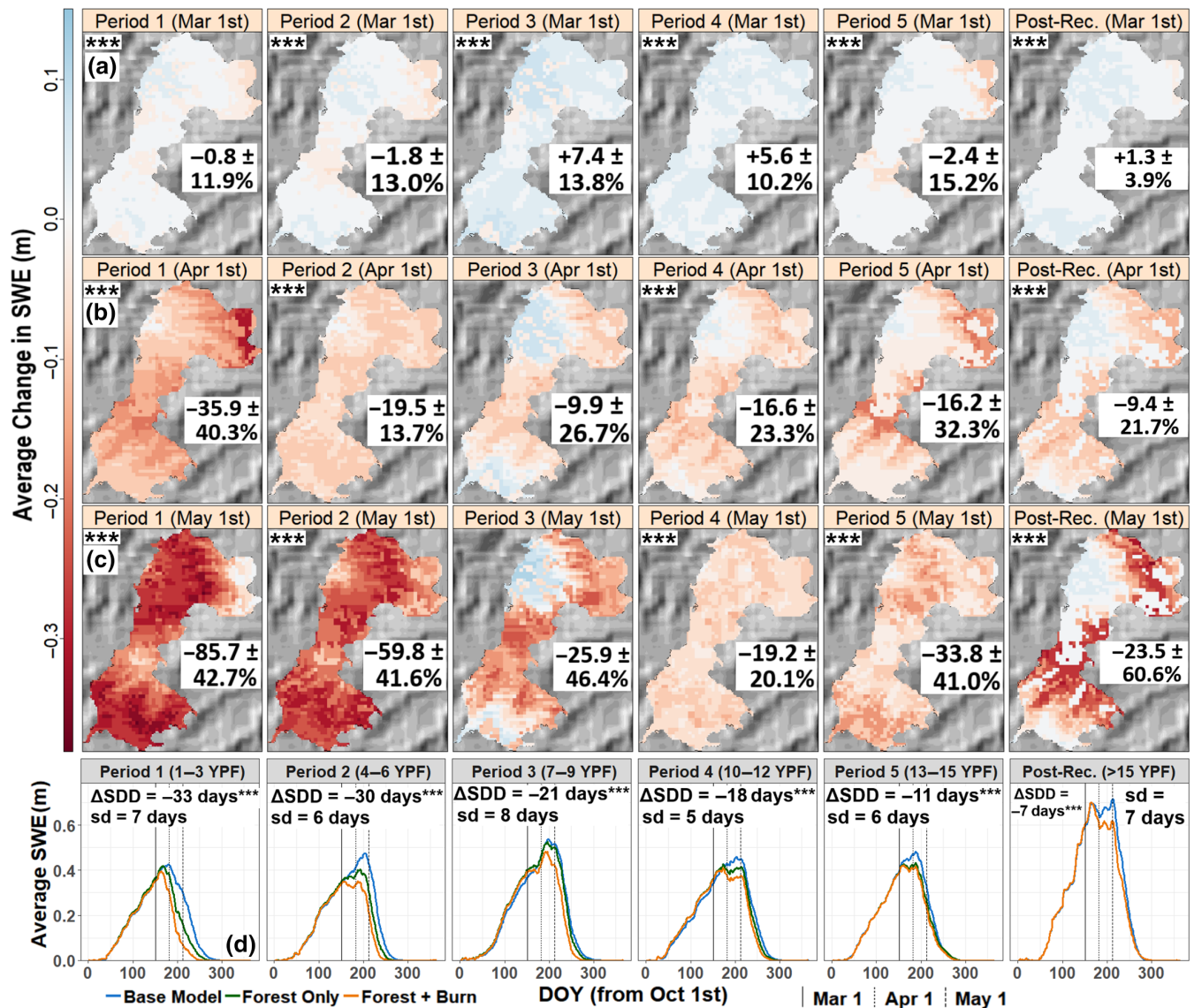


FIGURE 5 The change in snow-water equivalent depth (SWE) depth between the base model and postfire snow albedo recovery model in the Green Knoll fire (Ignition Year: 2001). Over 15 years of postfire recovery, postfire effects caused slight changes in SWE during March 1st (a), but then caused modest reductions in April 1st SWE (b), followed by profound reductions in May 1st (c). Postfire changes in SWE tended to reduce in magnitude over each successive recovery period, but, critically, post-recovery reductions in SWE were still present 16+ years (Post-Rec.) following fire (d).

SWE across the Roosevelt Fire substantially decreased ($\mu = -45.76\%$, $\sigma = 27.41\%$, $p < 0.001$; Table S3c) in the postfire snow albedo and forest structure recovery model relative to the base model (Figure 4c). Earlier melt onset and decreased average peak SWE in the Roosevelt Fire culminated in an advanced SDD by almost 1 month ($\mu = -29$ days, $\sigma = 5$ days; $p < 0.001$; Table 1) over the first 2 years immediately following fire included in the modelling period.

3.3 | Recovery of postfire effects on snow volume and snow disappearance date

Over the 15-year recovery period following fire, modelled postfire effects on snow albedo and forest structure steadily recovered, yet

associated decreased peak SWE and advanced timing of SDD persisted. Peak SWE reductions initiated immediately following fire, persisted from 1 to 6 years postfire, (1–3 years $\mu = -6.8\%$ to 4–6 years $\mu = -3.1\%$; $p < 0.001$; Table 1) and generally reductions in SWE further declined 7–9 years postfire, with this amplified decrease in SWE occurring in most fires 7–9 years postfire (4–6 years $\mu = -3.1\%$ to 7–9 years $\mu = -3.9\%$; $p < 0.001$; Table 1). Across all modelled burned forests, peak SWE reductions were most variable during this same period (4–6 years $\sigma = 13.4\%$; Table 1). Over the 15-year postfire recovery period, peak SWE reductions varied across individual burned forests (total 15 year range of -0.7% to -10.6% ; Table 1) likely due to heterogeneity in prefire landcover, postfire burn severity, and topography and relative associated snow-pack energy balance. Across the 15-year postfire recovery period,

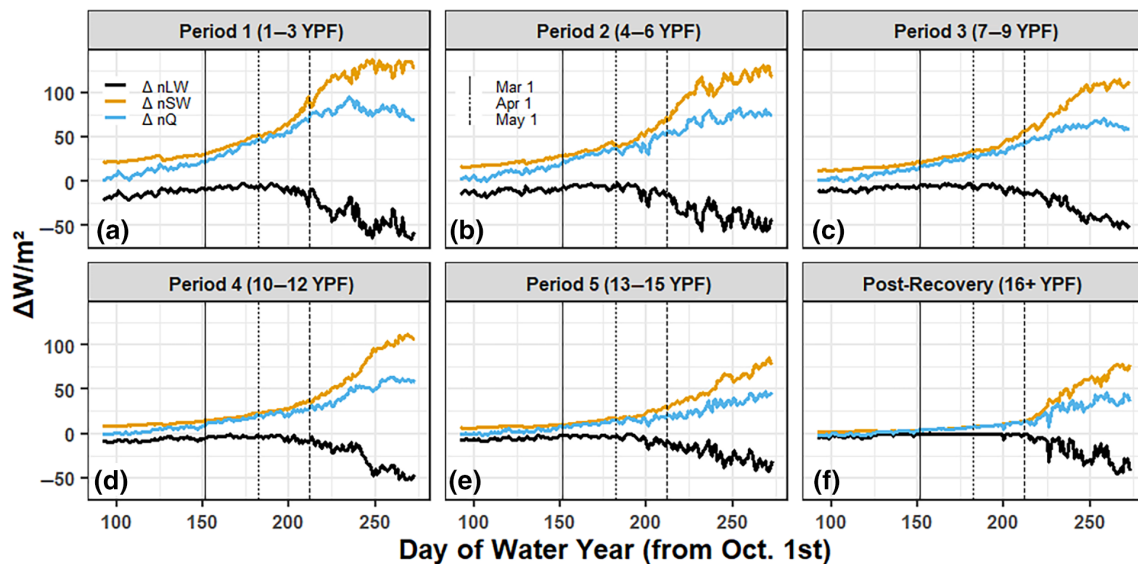


FIGURE 6 Difference between base model and postfire snow albedo and forest structure model net components of the snowpack energy balance averaged over 3-year bins since burn. The progressively more open postfire canopy allowed for increased solar shortwave incident on the snow surface over years since fire, but increasing snow albedo over years since fire drive the increases in internal snowpack energy and associated changes in snowpack volume. The difference in net shortwave inputs between models decreases over years since fire showing that postfire effects on snow albedo drive changes in peak snowpack volume over 15 years postfire and beyond.

average SWE increased during the accumulation period (March 1st range of $\mu = +2.4\%$ to $\mu = +7.2\%$, $p < 0.001$; Table S3a), average SWE was more variable during historical peak SWE (April 1st range of $\mu = +0.4\%$ to $\mu = -5.8\%$, $p < 0.001$; Table S3b), and average SWE decreased substantially during the ablation period (May 1st range of $\mu = -51.6\%$ to $\mu = -17.0\%$, $p < 0.001$; Table S3c) across all eight modelled burned forests.

As an example of long-term recovery and persistent postfire effects on snow-water storage and snowmelt timing, we focus on one large older modelled fire, the Green Knoll Fire, which burned in 2001. The Green Knoll fire occurred early during the modelling period and so provides a long-term perspective of modelled postfire effects on snow hydrology across the 15-year postfire recovery period and beyond. Over the 15-years following fire, changes in peak SWE in the Green Knoll Fire were consistent with the broader changes observed across most of the chronosequence of modelled burned forests. Over the 15-year recovery period, postfire effects on snow albedo and forest structure in the Green Knoll Fire reduced peak SWE substantially in the first few years following fire (peak SWE 1–3 years $\mu = -11.9\%$, $\sigma = 4.0\%$, $p < 0.001$; Table 1), and reductions in peak SWE persisted late into the postfire recovery period (peak SWE 13–15 years $\mu = -6.0\%$, $\sigma = 5.5\%$, $p < 0.001$; Table 1), and even beyond the postfire recovery period (peak SWE 16+ years $\mu = -2.5\%$, $\sigma = 4.1\%$, $p < 0.001$; Table 1). Over the 15-year recovery period, the greatest reduction in peak SWE in the Green Knoll Fire did not occur immediately but during the 4–6 year following fire period ($\mu = -14.93\%$, $\sigma = 4.43\%$, $p < 0.001$; Table 1).

Over the 15-year following fire recovery period, postfire effects on snow albedo and forest structure in the Green Knoll Fire produced

minimal change in accumulation season SWE (March 1st 1–3 years $\mu = -0.8\%$, $\sigma = 6.0\%$, $p < 0.001$; March 1st 13–15 years $\mu = -2.4\%$, $\sigma = 7.6\%$, $p < 0.001$; Table S3a). Accumulation period SWE (March 1st SWE) was similar between the postfire snow albedo and forest structure recovery model and the postfire forest structure model for all recovery years, indicating that snow accumulation may be controlled more by postfire forest structure than postfire snow albedo (Figure 5d). SWE decreased at the start of the ablation season (April 1st) in the postfire snow albedo and forest structure recovery model relative to the base model across the full 15-year recovery period (April 1st 1–3 years $\mu = -35.9\%$, $\sigma = 20.2\%$, $p < 0.001$; April 1st 13–15 years $\mu = -16.2\%$, $\sigma = 16.1\%$, $p = \text{ns}$; Table S3b). In the Green Knoll Fire, the greatest reductions in April 1st SWE occurred 1–6 years following fire. Across the entire 15-year postfire recovery period, SWE substantially decreased during the ablation season (May 1st) in the postfire snow albedo and forest structure recovery model (May 1st 1–3 years $\mu = -85.7\%$, $\sigma = 21.3\%$, $p < 0.001$; May 1st 13–15 years $\mu = -33.8\%$, $\sigma = 20.5\%$, $p < 0.001$; Table S3c). In the Green Knoll Fire, significant reductions ablation season SWE persisted across the entire 15-year postfire recovery period (Table S3c).

Over the 15-year postfire recovery period, cumulative modelled postfire effects on peak SWE in modelled fires summed to a profound total reduction in snow-water storage of almost 11 M m^3 ($\mu = -11.0 \text{ M m}^3$, $\sigma = 7.0 \text{ M m}^3$, $p < 0.001$; Table 1) or a 4.5% reduction ($\sigma = 11.4\%$, $p < 0.001$; Table 1), more than double the loss in snow-water storage in the first year following fire alone (4.3 M m^3 or 8.4%; $\sigma = 5.0 \text{ M m}^3$ or 9.4; $p < 0.001$; Table 1). Even after the 15-year postfire recovery period (16+ years postfire), peak

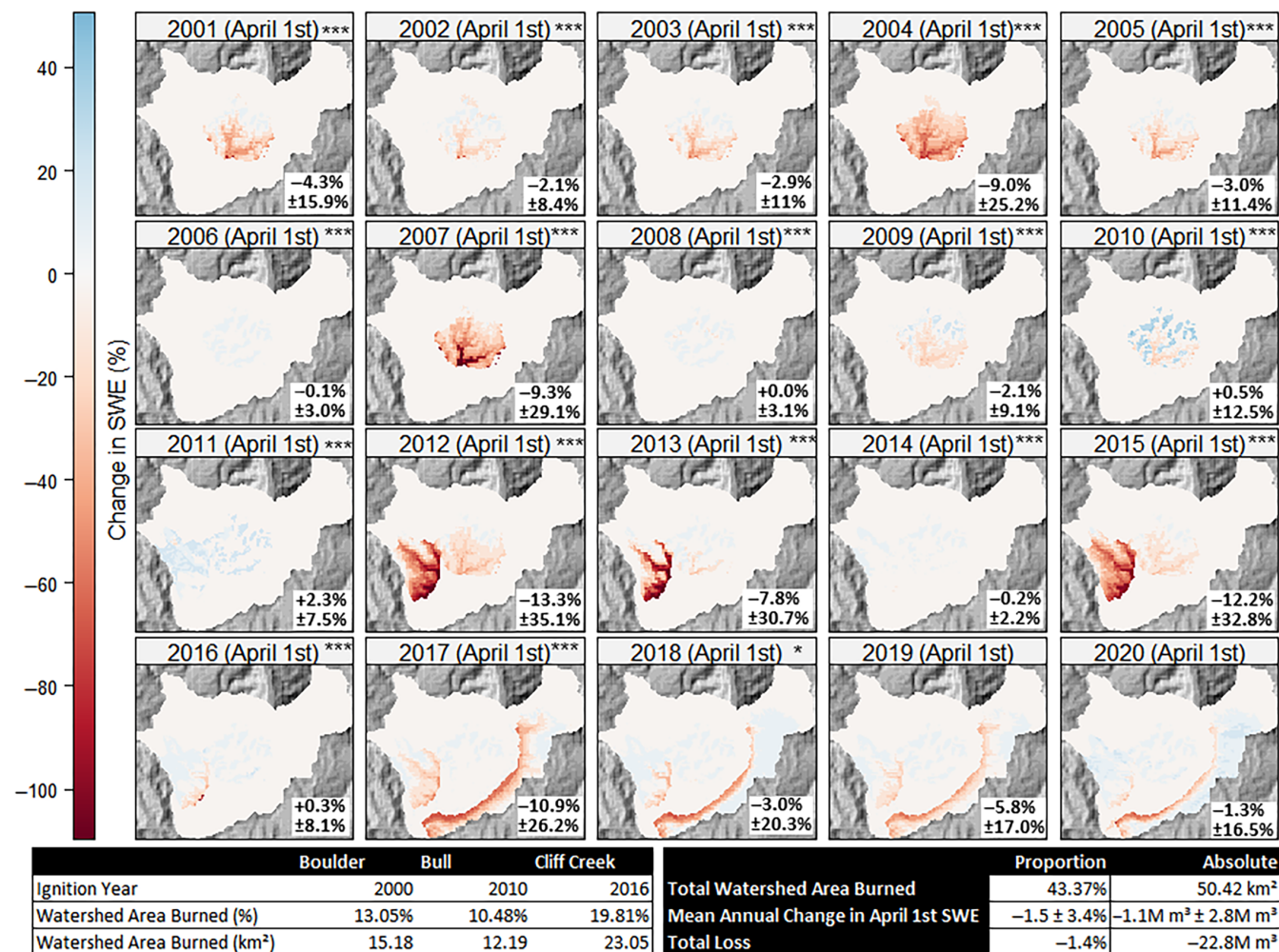


FIGURE 7 Watershed scale impacts of postfire effects and recovery in the Lower Granite Creek (LGC) subbasin during the ablation period (April 1st) for every year in the simulation. Postfire effects on snow albedo and forest structure caused net reductions in average April 1st SWE within the LGC subbasin in all but one year between 2000 and 2020, indicating that postfire effects on snow and forest structure cause lasting reductions in watershed-scale historical peak SWE for many years following fire.

SWE still persistently decreased in the Green Knoll Fire relative to the unburned base model ($\mu = -2.5\%$, $\sigma = 4.1\%$, $p < 0.001$; Table 1). Postfire effects on snow hydrology persisted during the post-recovery period (16+ years postfire) due to the transition in landcover. In the accumulation season (March 1st) SWE increased ($\mu = 1.3\%$, $p < 0.001$; Table S3a), at historical peak SWE (April 1st) SWE decreased ($\mu = -9.4\%$, $\sigma = 10.9\%$, $p < 0.001$; Table S3b), and during ablation (May 1st) SWE sharply decreased ($\mu = -23.5\%$, $\sigma = 30.3\%$, $p < 0.001$; Table S3c), due to the post recovery shift in snow albedo and forest structure resembling that of an open meadow (Figure 5b,c). Following the postfire recovery period (16+ years postfire), the postfire snow albedo had recovered over time to resemble that of an open meadow; therefore, persistent postfire effects on the net snowpack energy balance were primarily driven by increases in incoming shortwave as result of forest degradation (Figure 6f, Figure S1F).

Reductions in ablation season SWE (April 1st and May 1st) occurred in concert with earlier snowmelt onset, typically prior to

April 1st under postfire conditions, but after April 1st under unburned forest conditions (Figure 5d). Snow-water storage in the postfire snow albedo and forest structure recovery model diverged from the postfire forest structure model during peak SWE (April 1st) across 1 to 12 years following fire, with the postfire forest structure model continuing to accumulate snow beyond April 1st (Figure 5d). Ablation season postfire snowpack energy balance was dominated by net snowpack shortwave radiation (SW $\mu = 0.1$ – 27.6 Wm^{-2} , LW $\mu = 0.0$ – 6.0 Wm^{-2} ; Tables S4 and S5; Figure 6). Postfire net snowpack shortwave radiation increased immediately following fire, as a result of both postfire reductions in snow albedo and postfire forest canopy degradation (ablation season $\Delta n\text{SW}_{\text{forest}} \mu = 37.1 \text{ Wm}^{-2}$, $\sigma = 12.5 \text{ Wm}^{-2}$, $\Delta n\text{SW}_{\text{albedo}} \mu = 27.6 \text{ Wm}^{-2}$, $\sigma = 17.3 \text{ Wm}^{-2}$; Table S4; Figure 6). However, over the 15-year postfire recovery period postfire forest degradation accounted for the majority of postfire radiative forcing on snow (ablation season $\Delta n\text{SW}_{\text{forest}}$ range of 54.0%–21.3%, $\Delta n\text{SW}_{\text{albedo}}$ range of 28.7% to 0.21%; Table S4; Figure 6).

3.4 | Effects of postfire impacts and recovery at the watershed scale

Watershed-scale postfire effects on snow albedo and forest structure recovery across the Lower Granite Creek (LGC) subbasin aggregated into persistent reductions in snow–water storage in the ablation season (April 1st). Cumulative postfire effects on snow hydrology in the LGC subbasin at historical peak SWE decreased annual snow–water storage volume over the 20-year modelling period ($\mu = -1.5\%$, $\sigma = 3.4\%$, $p < 0.001$), and the greatest proportional losses in SWE occurred during 2012 and 2017 (2012 SWE, $\mu = -13.3\%$, $\sigma = 17.0\%$, $p < 0.001$; 2017 SWE, $\mu = -10.9\%$, $\sigma = 13.1\%$, $p < 0.001$) (Figure 7). During 2012, postfire effects from the Boulder (12 years postfire) and Bull Fires (2 years postfire) combined to produce reductions in snow–water storage volume across the LGC subbasin. While during 2017, postfire effects from the Cliff Creek (1 year postfire) and Bull Fires (7 years postfire) combined to produce the reduction in snow–water storage volume across the LGC subbasin (Figure 7). Burned forests even late in their postfire recovery reduced SWE and contributed to enhanced SWE reductions in recently burned forests cumulatively across the watershed. Frequent and extensive forest fires within the LGC subbasin and the associated postfire effects on snow albedo and forest structure resulted in a modest total reduction at the time of historical peak SWE (April 1st) over the 20-year modelling period (a total volume of $>22 \text{ M m}^3$ or 1.5% of additional snowmelt during historical peak SWE) (Figure 7).

The greatest reductions in watershed-scale SWE however were observed during the ablation season (May 1st). Postfire effects on snow hydrology during ablation season decreased annual snow–water storage volume far more than at historical peak SWE (May 1st: $\mu = -6.30\%$, $\sigma = 3.43\%$, $p < 0.001$; April 1st: $\mu = -1.5\%$, $\sigma = 3.4\%$, $p < 0.001$; Figure S4). Further, the greatest proportional losses in ablation season SWE occurred at different times than at historical peak SWE (2015 SWE, $\mu = -9.5\%$, $\sigma = 32.0\%$, $p < 0.001$; 2017 SWE, $\mu = -14.58\%$, $\sigma = 38.1\%$, $p < 0.001$; Figure S4) indicating that, at the watershed scale, timing of postfire reductions in SWE is highly variable even within the same snow season. In total, forest fires within the LGC subbasin resulted in a profound total reduction in ablation season SWE (May 1st) over the 20-year modelling period (a total volume of $>94 \text{ M m}^3$ or 5.85% of additional snowmelt during ablation season; Figure S4), far more than the SWE reductions that occurred at historical peak SWE (a total volume of $>22 \text{ M m}^3$ or 1.5% of additional snowmelt during historical peak SWE; Figure S4).

3.5 | Model and measurement comparison

Evaluation of modelled SWE results with in-situ SWE measurements collected in several of the burned forests demonstrates an overestimated SWE in both the base model ($\mu = +40.22\%$, $\sigma = 19.44\%$; Table 2) and postfire snow albedo and forest structure recovery model ($\mu = +41.61$, $\sigma = 23.15\%$; Table 2) and both models were relatively close in accuracy ($<1.5\%$ difference; Table 2). The comparison

of the few point-based measurements collected in the field to spatially distributed 100 m^2 spatial resolution model results highlight the difficulty of comparisons across scales and emphasize the importance of evaluating relative changes of postfire volumetric estimates between the base model, postfire forest structure recovery model, and postfire snow albedo and forest structure recovery model.

4 | DISCUSSION

Modelling the immediate and persistent postfire effects on snow albedo and forest structure degradation over the 15-year postfire recovery period using best estimate postfire parameterizations provided volumetric watershed-scale estimates of postfire changes in snow–water storage and snowmelt timing. Over the 15-year postfire recovery period across the modelled chronosequence of eight burned forests, peak SWE decreased by over 4% and SDD advanced by over a week on average (Table 1). Sustained shifts in postfire snow–water storage and snowmelt timing have the capacity to decrease downstream minimum streamflow (Godsey et al., 2014; Hallema et al., 2018), advance the timing of peak streamflow (Wieder et al., 2022), reduce spring and summertime soil moisture (Harpold, 2016; Westerling, 2016), extend vegetation growing seasons, and increase risk of future forest fire (Abatzoglou & Kolden, 2013; Westerling, 2016). Our modelled estimates discussed here highlight the importance of understanding immediate and lasting postfire effects and recovery of snow–water storage and snowmelt timing and inform future water resource management in burned forested snow-dominated watersheds.

4.1 | Immediate postfire effects on snow hydrology

In the winter immediately following fire, postfire darkening of snow albedo and forest structure degradation reduced peak SWE by over 8% and advanced SDD by over a month (Table 1). These modelled postfire changes were driven by earlier melt onset from increased postfire shortwave radiative forcing on snow heightened during the spring ablation season (Figure S2; Figure 6). In the more open postfire forest canopy, snow accumulation increased slightly during March, but earlier melt onset reduced snow–water storage in April and even further in May (Figure 4d). Immediately following fire, the modelled postfire reduction in snow–water storage was amplified during spring with heightened postfire snow albedo darkening, increased incoming solar radiation, and warmer spring temperatures (Figure 4c,d; Figure 6). Interannual climate variability likely influenced overall variability in postfire snow hydrology metrics as the years included in modelled immediate and recovery postfire periods varied across the chronosequence depending on the year of ignition for each burned forest. Later and higher magnitude peak SWE seemed to buffer postfire effects on snow based on observation of average SWE within burn regions (Figure 5d); however, further analysis on how factors

Fire	Base model Avg. % error (%)	SD (%)	Postfire snow albedo model		n
			Avg. % error (%)	SD (%)	
Horsethief Canyon	+61.06	—	+58.64	—	1
Bull	+24.67	16.62	+23.03	16.9	16
Boulder	+40.71	11.02	+41.22	11.15	9
Cliff Creek	+40.4	13.47	+41.17	9.765	13
Lava Mountain	+48.89	12.04	+46.18	15.13	8
Roosevelt	+59.79	13.42	+67.89	11.96	13
Overall	+40.22	19.44	+41.61	23.15	60

TABLE 2 Results of the model validation using field measurements of SWE collected from six of the burns between February and March of 2019. Percent error between the base/postfire albedo model were calculated against the field observations and the standard deviation was included when $n > 1$. Instances where the postfire snow albedo model performed better than the base model are in bold.

such as precipitation, date of peak SWE, and others influence the resulting magnitude of postfire changes in snow hydrology will be needed to confirm this.

4.2 | Recovery of postfire effects on snow hydrology

Over the 15-year postfire recovery period, modelled reductions in snow–water storage persisted across the chronosequence of eight burned forests for the entire 15-year postfire recovery period (Table 1). Increases in net shortwave radiative forcing from the more open forest canopy and darkening of snow albedo continued to dominate changes in snowpack energy balance for the entire postfire recovery period (Figure 6). Earlier melt onset led to advanced snow disappearance date across the chronosequence of burned forests for the entire 15-year postfire recovery period (Δ SDD range of -31 to -8 days; Table 1) and even beyond into the post-recovery period (16+ years postfire Δ SDD -5 days; Table 1). Modelled estimates of postfire effects on snow–water storage and snow disappearance date were consistent with previous empirical analyses of 80 burned SNOTEL sites across the western US (Smoot & Gleason, 2021). Smoot and Gleason (2021) documented postfire reductions of SWE of 0.15 to 0.05 m over 10 years following fire, similar to modelled results of approximately 0.02 m reductions from this study 10–12 years postfire (Table 1). Smoot and Gleason (2021) reported an advancement of SDD of -7 to -14 days over 10 years following fire, similar to advancements of modelled SDD of -17 days 10–12 years following fire (Table 1). In other studies, snow disappearance date advanced 8 days and peak SWE decreased 5.7% on average following fire across burned SNOTEL sites in the middle Rockies (Giovando & Niemann, 2022), similar trends to our modelled results for SDD change 13+ years following fire (-8 days; Table 1) and our average SWE change over 15 years following fire (-4.5% ; Table 1). Advanced snow disappearance date and lower magnitude peak SWE following fire has been shown to occur in other regions across the western US and have been shown to be driven by postfire canopy reduction and additional shortwave radiative forcing that we modelled here (Hatchett et al., 2023; Kampf et al., 2022; Micheletty et al., 2014).

Across the chronosequence of eight burned forests in western Wyoming, modelled SWE and SDD metrics were variable over the

15-year postfire recovery period. These results highlight the difficulty in predicting the degree to which snow–water storage will be affected in burned watersheds over many years following fire, even when we assume uniform burn patterns over forest fires occurring within a narrow scope of landscape and climate variability. Many regions in the western United States rely on predictable spring runoff afforded by ample snow–water storage (Li et al., 2017; Liu et al., 2022). The variability of postfire snow hydrology responses seen across our study compound with the spatial and climatic variability present across the western United States and increasing interannual variability in runoff timing due to the effects of climate change on snow–water storage and snowmelt timing (Li et al., 2017; Wieder et al., 2022).

4.3 | Watershed-scale postfire effects on snow hydrology

Postfire effects on snow hydrology integrated across the Lower Granite Creek watershed reduced snow water storage, accelerated snowmelt onset, and advanced snow disappearance date, which persisted across the 20-year modelling period (Figure 7). Cumulative postfire effects on snow albedo and forest structure from the three burned forests (Boulder, Bull and Cliff Creek Fires) reduced historical peak snow–water storage (April 1) across the watershed over most of the 20-year modelling period (Figure 7). Modelled trends in postfire recovery of snow–water storage were consistent from individual burned forests to the watershed-scale, with the greatest postfire reductions in snow–water storage volume occurring approximately 1 to 3 years following each forest fire ignition in the basin. Earlier peak SWE following fire due to earlier postfire snowmelt onset across the watershed led to modest losses of snow–water storage in spring (Δ SWE $\mu = -1.1$ M m³, $\sigma = 1.4$ M m³ on average per year). Over 20 years, this resulted in a modest cumulative total loss of spring snow–water storage (Δ SWE $\mu = -22.8$ M m³) relative to unburned forest conditions (Figure 7). However, at ablation season closer in time to when snow storage converts to streamflow, cumulative reductions in SWE over 20 years resulted in a much more substantial loss in late spring snow–water storage (Δ SWE $\mu = 94$ M; Figure S4). As a frame of reference, this modelled annual postfire reduction in spring snow–water storage is the equivalent of 20% of the total annual average streamflow volume measured at the USGS stream gage at the

outlet of the Lower Granite Creek subbasin (USGS 13019438) of 29 M m³ between 1982 and 1993 (U.S. Geological Survey National Geospatial Program, 2022). Yet, it is likely these modelled estimates are conservative and actually underestimating the full extent of post-fire effects on snow over the postfire recovery period as reductions in snow–water storage persist beyond the 20-year modelling period for individual fires in the watershed. Changes in ablation season (May 1st) and historical peak SWE (April 1st) were still apparent as late as 2020 in the Boulder Fire, 4 years following the end of the postfire recovery period. Postfire effects over the entire 15-year postfire recovery period from the Bull and Cliff Creek Fires (burned in 2010 and 2016) were not fully captured in the modelling extent (Figure 7; Figure S4).

As forest fires increase across the western US, it is increasingly important we understand immediate and persistent postfire effects on snow–water storage and snow–water resource availability across burned forested watersheds. Multiple studies have demonstrated that reductions in peak snow volume can alter summer low flows (Godsey et al., 2014; Jenicek et al., 2018), especially in cold and dry continental snow zones (Hammond et al., 2018), and that annual river flow can be altered in watersheds burned over as little as 19% of their area (Hallema et al., 2018). The modelled estimates of postfire effects on snow–water storage presented here highlight the potential for forest fires to markedly alter resulting annual streamflow runoff volume and timing for decades following fire (Godsey et al., 2014; Williams et al., 2022). Our findings provide volumetric, spatially-distributed, time varying, process-based estimates of postfire effects on snow hydrology and recovery over decades following fire and inform water resource management for better estimates of postfire effects on snow hydrology and the associated the timing and volume of water resource availability.

4.4 | Model evaluation

According to limited in situ SWE measurements, the base model, the postfire forest structure, and postfire snow albedo and forest structure model similarly overestimated SWE (base model SWE difference $\mu = +40.22\%$, $\sigma = 19.44\%$; postfire snow albedo and forest structure model SWE difference $\mu = +41.61\%$, $\sigma = 23.15\%$; Table 2) in the individual burned forests. The sparse field measurements were limited in scope and therefore not effective to evaluate exact modelled estimates. Likely the differences between modelled SWE results and field SWE measurements were due to the offset seasonality of field measurements, the disparity in spatial resolution, and the time range between the two datasets. For these reasons, we focused the discussion on the relative postfire effects on snow–water storage and snowmelt timing between the base model, the postfire forest structure model, and the postfire snow albedo and forest structure model. We acknowledge our conservative approach to postfire snow albedo and forest structure modelling, and these in situ measurement comparisons, emphasize we may be underestimating postfire effects on snow–water storage in our modelled estimates relative to measurements.

Field measurements of SWE were taken during early winter (February and March of 2019 and 2020). Changes in modelled SWE due to postfire effects were minor or near zero during the accumulation season (Figure 4a; Figure 5a), which explained why the base model and postfire snow albedo model had similar evaluation statistics compared to measurements (Table 2). We expected that if the field measurements had been taken later in the season near or after peak SWE when the postfire models showed the greatest reductions in SWE, modelled estimates would likely be much closer to field SWE measurements. Further, the small spatial area and time frame in which the field data were collected due to accessibility, made these data inadequate for evaluating our spatial and temporally extensive modelled results. For example, the field measurements for each burned forest were collected in a small area and over the course of only 5 weeks in a single year. In contrast, the modelled results span thousands of square kilometres, multiple decades, and were spatially-distributed in grids of 100 m². Although the model tended to overestimate SWE at the field validation sites, the model showed good agreement with 20 years of continuous SWE data from SNOTEL sites located within the model domain (Table S2) supporting the relative estimates of postfire effects on snow over the broad spatial and time scales investigated in this study. In addition, the changes in modelled postfire SWE and SDD over 10 years following fire are consistent with SWE and SDD observations at burned SNOTEL sites across the region (Smoot & Gleason, 2021).

4.5 | Uncertainties in model estimates of postfire effects on snow hydrology

We incorporated best estimate postfire parameterizations of snow albedo and forest structure recovery, in a reliable and well-tested physically-based spatially-distributed snow evolution model, which extended existing postfire snow albedo and forest structure algorithms over decades following fire. The 15-year recovery period was consistent with work from Gersh et al. (2022), Gleason et al. (2019) and Smoot and Gleason (2021) which all evaluated forest fire effects on snow hydrology in the Rocky Mountains and beyond. However, the postfire effects on snow albedo parameterizations were based on empirically-derived algorithms initially developed in the western Oregon Cascades to model postfire effects on snow hydrology, a different snow climate than the Rocky Mountains (Gleason & Nolin, 2016). Our postfire parameterization of forest structure linearly represented forest degradation over the 15-year postfire recovery period, while previous work showed that delayed tree mortality and forest degradation can occur at an exponentially decaying rate following fire (Angers et al., 2011; J. K. Brown & DeByle, 1987; Dunn & Bailey, 2012) and can depend on many factors such as seed supply, distance to sources, and pre- and postfire climate (Stevens-Rumann & Morgan, 2019).

As observed from in-situ forest structure observations (Figure 2) and remote sensing data (Gersh et al., 2022), the 15-year postfire recovery period included in these parameterizations of postfire snow albedo and forest structure recovered from a recently burned

coniferous forest to an open meadow. These postfire snow albedo and forest structure recovery parameterizations build upon previous models of postfire snow hydrology (Gleason & Nolin, 2016) by extending the immediate forest fire effects across 15-years following forest fire. This work, modelling the lasting postfire effects on snow hydrology over decades following fire, provides an integrated perspective of persistent and cumulative impacts of burned forests on snow–water storage and snowmelt timing; however, we recognize this is not the end of postfire forest recovery which continues beyond the 20-year modelling period. Future modelling work needs to further improve forest structure parameterizations to capture the complete postfire recovery through informed potential forest regeneration scenarios back to antecedent prefire conditions. Our model parameterizations make meaningful strides towards more representative modelling of the recovery of postfire effects on snow hydrology. Future expansions and specificity of this work will further improve the accuracy of estimates of complete postfire recovery of snow albedo and forest structure and lasting postfire effects on snow hydrology across burned forested watersheds.

5 | CONCLUSIONS

Burned forests darken snow albedo as the postfire forest structure degrades following fire, increasing the postfire shortwave radiative forcing on snow, decreasing snow–water storage, advancing snowmelt timing, and potentially altering downstream water availability over decades following fire. This study evaluated the immediate and persistent postfire effects on snow–water storage and snowmelt timing by incorporating best estimate postfire snow albedo and forest structure recovery parameterizations in a spatially-distributed physically-based snow mass and energy balance model. We estimated relative postfire effects on snow albedo and forest structure, and the recovery of peak SWE, SDD, and seasonal SWE volume reductions over a chronosequence of eight burned forests over 20 years following fire.

Immediately following forest fire, snow–water storage increased by up to 7% in winter, but decreased by 6% near peak SWE, and up to 52% in spring, while earlier melt onset advanced snow disappearance date by over 30 days. Over the 15-year postfire recovery period, forest fire effects on snow albedo and forest structure, reduced snow–water storage by 4.5% overall, an additional 25.8% above the immediate postfire effects in the first year following fire alone. After the 15-year postfire recovery period, forest fire effects on snow albedo and forest structure persisted with continued reductions in snow–water storage of 0.30% and a 5-day earlier snow disappearance date. Continued modelling work is required to extend these estimates to represent the complete postfire recovery of snow albedo and forest structure after the 20 years following fire for the Triple Divide region of western Wyoming and beyond to the western US.

Immediate and persistent forest fire effects on snow–water storage and snowmelt timing were consistent across the chronosequence of eight burned forests and cumulative across a burned forested watershed for decades following fire. The modelled results of this study highlight

that forest fires have immediate, profound, and lasting effects on snow–water storage, snowmelt timing, and likely downstream water resource availability that last decades beyond the initial forest fire disturbance with hydrological implications beyond the forest fire perimeter. Volumetric watershed-scale estimates of postfire changes in snow–water storage and snowmelt timing are critical to our understanding of the immediate and lasting impacts of forest fires on the quantity and timing snow–water resource availability across the western US.

ACKNOWLEDGEMENTS

This research was funded by NASA as part of the Terrestrial Hydrology Program (Award #80NSSC19K0002). Special thanks to Glen Liston for his support in running SnowModel and troubleshooting our modifications and to Ryan Crumley for his support in initializing SnowModel. Open Access Funding provided by Portland State University Library.

DATA AVAILABILITY STATEMENT

The data that support the findings of this study are openly available in Google Drive at https://pdxscholar.library.pdx.edu/esm_data/5/.

ORCID

A. Surunis  <https://orcid.org/0009-0009-9853-4214>

REFERENCES

- Abatzoglou, J. T., & Kolden, C. A. (2013). Relationships between climate and macroscale area burned in the western United States. *International Journal of Wildland Fire*, 22(7), 1003. <https://doi.org/10.1071/WF13019>
- Abatzoglou, J. T., & Williams, A. P. (2016). Impact of anthropogenic climate change on wildfire across western US forests. *Proceedings of the National Academy of Sciences*, 113(42), 11770–11775. <https://doi.org/10.1073/pnas.1607171113>
- Alonso-González, E., Revuelto, J., Fassnacht, S. R., & Ignacio López-Moreno, J. (2022). Combined influence of maximum accumulation and melt rates on the duration of the seasonal snowpack over temperate mountains. *Journal of Hydrology*, 608, 127574. <https://doi.org/10.1016/j.jhydrol.2022.127574>
- Angers, V. A., Gauthier, S., Drapeau, P., Jayen, K., & Bergeron, Y. (2011). Tree mortality and snag dynamics in north American boreal tree species after a wildfire: A long-term study. *International Journal of Wildland Fire*, 20(6), 751. <https://doi.org/10.1071/WF10010>
- Barnett, T. P., Adam, J. C., & Lettenmaier, D. P. (2005). Potential impacts of a warming climate on water availability in snow-dominated regions. *Nature*, 438(7066), 303–309. <https://doi.org/10.1038/nature04141>
- Brown, J. K., & DeByle, N. V. (1987). Fire damage, mortality, and suckering in aspen. *Canadian Journal of Forest Research*, 17(9), 1100–1109. <https://doi.org/10.1139/x87-168>
- Brown, O. L. I. (1951). The Clausius-Clapeyron equation. *Journal of Chemical Education*, 28(8), 428. <https://doi.org/10.1021/ed028p428>
- Buchhorn, M., Lesiv, M., Tsendbazar, N. E., Herold, M., Bertels, L., & Smets, B. (2020). Copernicus global land cover layers—collection 2. *Remote Sensing*, 12(6), 1044.
- Burles, K., & Boon, S. (2011). Snowmelt energy balance in a burned forest plot, Crownsnest pass, Alberta, Canada. *Hydrological Processes*, 25(19), 3012–3029.
- Busby, S. U., Moffett, K. B., & Holz, A. (2020). High-severity and short-interval wildfires limit forest recovery in the Central Cascade Range. *Ecosphere*, 11(9), e03247. <https://doi.org/10.1002/ecs2.3247>

- Cline, D. W. (1997). Snow surface energy exchanges and snowmelt at a continental, midlatitude alpine site. *Water Resources Research*, 33(4), 689–701. <https://doi.org/10.1029/97WR00026>
- Coop, J. D., Massatti, R. T., & Schoettle, A. W. (2010). Subalpine vegetation pattern three decades after stand-replacing fire: Effects of landscape context and topography on plant community composition, tree regeneration, and diversity. *Journal of Vegetation Science*, 21(3), 472–487. <https://doi.org/10.1111/j.1654-1103.2009.01154.x>
- Danielson, J. J., & Gesch, D. B. (2011). *Global multi-resolution terrain elevation data 2010 (GMTED2010) (No. 2011-1073)*. US Geological Survey.
- Dennison, P. E., Brewer, S. C., Arnold, J. D., & Moritz, M. A. (2014). Large wildfire trends in the western United States, 1984–2011. *Geophysical Research Letters*, 41(8), 2928–2933. <https://doi.org/10.1002/2014GL059576>
- Dunn, C. J., & Bailey, J. D. (2012). Temporal dynamics and decay of coarse wood in early seral habitats of dry-mixed conifer forests in Oregon's eastern cascades. *Forest Ecology and Management*, 276, 71–81. <https://doi.org/10.1016/j.foreco.2012.03.013>
- Esri Inc. (2022). “2D, 3D & 4D GIS Mapping Software/ArcGIS Pro.”. <https://www.esri.com/en-us/arcgis/products/arcgis-pro/overview>
- Fassnacht, S. R., & López-Moreno, J. I. (2020). Patterns of trends in niveograph characteristics across the western United States from snow telemetry data. *Frontiers of Earth Science*, 14(2), 315. <https://doi.org/10.1007/s11707-020-0813-5>
- Finco, M., Quayle, B., Zhang, Y., Lecker, J., Megown, K. A., & Brewer, C. K. (2012). “Monitoring trends and burn severity (MTBS): Monitoring wildfire activity for the past quarter century using landsat data.”. Morin, Randall S.; Liknes, Greg C., comps. Moving from status to trends: Forest inventory and analysis (FIA) symposium 2012; 2012 December 4–6; Baltimore, MD. Gen. Tech. Rep. NRS-P-105, Newtown Square, PA: U.S. Department of Agriculture, Forest Service, Northern Research Station [CD-ROM].
- Frankson, R., Kunkel, K. E., Stevens, L. E., Easterling, D. R., Stewart, B. C., Umphlett, N. A., & Stiles, C. J. (2022). “Wyoming state climate summary 2022.”. (NOAA technical report NESDIS 150-WY; p. 5) NOAA/NESDIS, Silver Spring, MD.
- Garvelmann, J., Pohl, S., & Weiler, M. (2014). Variability of observed energy fluxes during rain-on-snow and clear sky snowmelt in a Midlatitude Mountain environment. *Journal of Hydrometeorology*, 15(3), 1220–1237. <https://doi.org/10.1175/JHM-D-13-0187.1>
- Gersh, M., Gleason, K. E., & Surunis, A. (2022). Forest fire effects on landscape snow albedo recovery and decay. *Remote Sensing*, 14(16), 4079. <https://doi.org/10.3390/rs14164079>
- Giovando, J., & Niemann, J. D. (2022). Wildfire impacts on snowpack phenology in a changing climate within the Western U.S. *Water Resources Research*, 58(8), e2021WR031569. <https://doi.org/10.1029/2021WR031569>
- Gleason, K. E., McConnell, J. R., Arienzo, M. M., Chellman, N., & Calvin, W. M. (2019). Four-fold increase in solar forcing on snow in western U.S. burned forests since 1999. *Nature Communications*, 10(1), 2026. <https://doi.org/10.1038/s41467-019-09935-y>
- Gleason, K. E., & Nolin, A. W. (2016). Charred forests accelerate snow albedo decay: Parameterizing the post-fire radiative forcing on snow for three years following fire. *Hydrological Processes*, 30(21), 3855–3870. <https://doi.org/10.1002/hyp.10897>
- Gleason, K. E., Nolin, A. W., & Roth, T. R. (2013). Charred forests increase snowmelt: Effects of burned woody debris and incoming solar radiation on snow ablation: Charred forests increase snowmelt. *Geophysical Research Letters*, 40(17), 4654–4661. <https://doi.org/10.1002/grl.50896>
- Godsey, S. E., Kirchner, J. W., & Tague, C. L. (2014). Effects of changes in winter snowpacks on summer low flows: Case studies in the Sierra Nevada, California, USA. *Hydrological Processes*, 28(19), 5048–5064. <https://doi.org/10.1002/hyp.9943>
- Gorelick, N., Hancher, M., Dixon, M., Ilyushchenko, S., Thau, D., & Moore, R. (2017). Google earth engine: Planetary-scale geospatial analysis for everyone. *Remote Sensing of Environment*, 202, 18–27. <https://doi.org/10.1016/j.rse.2017.06.031>
- Hale, K. E., Wlostowski, A. N., Badger, A. M., Musselman, K. N., Livneh, B., & Molotch, N. P. (2022). Modeling streamflow sensitivity to climate warming and surface water inputs in a montane catchment. *Journal of Hydrology: Regional Studies*, 39, 100976. <https://doi.org/10.1016/j.ejrh.2021.100976>
- Hallema, D. W., Sun, G., Caldwell, P. V., Norman, S. P., Cohen, E. C., Liu, Y., Bladon, K. D., & McNulty, S. G. (2018). Burned forests impact water supplies. *Nature Communications*, 9(1), 1307. <https://doi.org/10.1038/s41467-018-03735-6>
- Hammond, J. C., Saavedra, F. A., & Kampf, S. K. (2018). How does snow persistence relate to annual streamflow in mountain watersheds of the Western U.S. with wet maritime and dry continental climates? *Water Resources Research*, 54(4), 2605–2623. <https://doi.org/10.1002/2017WR021899>
- Harpold, A. A. (2016). Diverging sensitivity of soil water stress to changing snowmelt timing in the Western U.S. *Advances in Water Resources*, 92, 116–129. <https://doi.org/10.1016/j.advwatres.2016.03.017>
- Harpold, A. A., Biederman, J. A., Condon, K., Merino, M., Korgaonkar, Y., Nan, T., Sloat, L. L., Ross, M., & Brooks, P. D. (2014). Changes in snow accumulation and ablation following the las Conchas Forest fire, New Mexico, USA. *Ecohydrology*, 7(2), 440–452. <https://doi.org/10.1002/eco.1363>
- Harvey, B. J., Donato, D. C., & Turner, M. G. (2016). High and dry: Post-fire tree seedling establishment in subalpine forests decreases with post-fire drought and large stand-replacing burn patches. *Global Ecology and Biogeography*, 25(6), 655–669. <https://doi.org/10.1111/geb.12443>
- Hatchett, B. J., Koshkin, A. L., Guirguis, K., Rittger, K., Nolin, A. W., Heggli, A., Rhoades, A. M., East, A. E., Siirila-Woodburn, E. R., Brandt, W. T., Gershunov, A., & Haleakala, K. (2023). Midwinter dry spells amplify post-fire snowpack decline. *Geophysical Research Letters*, 50(3), e2022GL101235. <https://doi.org/10.1029/2022GL101235>
- Hiemstra, C. A., Liston, G. E., & Reiners, W. A. (2006). Observing, modeling, and validating snow redistribution by wind in a Wyoming upper treeline landscape. *Ecological Modelling*, 197(1–2), 35–51. <https://doi.org/10.1016/j.ecolmodel.2006.03.005>
- Jenicek, M., Seibert, J., & Staudinger, M. (2018). Modeling of future changes in seasonal snowpack and impacts on summer low flows in alpine catchments. *Water Resources Research*, 54(1), 538–556. <https://doi.org/10.1002/2017WR021648>
- Kampf, S. K., McGrath, D., Sears, M. G., Fassnacht, S. R., Kiewiet, L., & Hammond, J. C. (2022). Increasing wildfire impacts on snowpack in the western U.S. *Proceedings of the National Academy of Sciences*, 119(39), e2200333119. <https://doi.org/10.1073/pnas.2200333119>
- Li, D., Wrzesien, M. L., Durand, M., Adam, J., & Lettenmaier, D. P. (2017). How much runoff originates as snow in the western United States, and how will that change in the future? *Geophysical Research Letters*, 44(12), 6163–6172. <https://doi.org/10.1002/2017GL073551>
- Liston, G. E., & Elder, K. (2006a). A distributed snow-evolution modeling system (SnowModel). *Journal of Hydrometeorology*, 7(6), 1259–1276. <https://doi.org/10.1175/JHM548.1>
- Liston, G. E., & Elder, K. (2006b). A meteorological distribution system for high-resolution terrestrial modeling (MicroMet). *Journal of Hydrometeorology*, 7(2), 217–234. <https://doi.org/10.1175/JHM486.1>
- Liston, G. E., Haehnel, R. B., Sturm, M., Hiemstra, C. A., Berezovskaya, S., & Tabler, R. D. (2007). Simulating complex snow distributions in windy environments using SnowTran-3D. *Journal of Glaciology*, 53(181), 241–256. <https://doi.org/10.3189/172756507782202865>

- Liston, G. E., & Hall, D. K. (1995). An energy-balance model of lake-ice evolution. *Journal of Glaciology*, 41(138), 373–382. <https://doi.org/10.3189/S0022143000016245>
- Liu, Q., Yang, Y., Liang, L., Yan, D., Wang, X., Li, C., & Sun, T. (2022). Hydrological effects of the snow fraction and its ecohydrological explication within the Budyko framework. *Journal of Hydrology*, 610, 127813. <https://doi.org/10.1016/j.jhydrol.2022.127813>
- Luce, C. H., Abatzoglou, J. T., & Holden, Z. A. (2013). The Missing Mountain water: Slower westerlies decrease orographic enhancement in the Pacific Northwest USA. *Science*, 342(6164), 1360–1364. <https://doi.org/10.1126/science.1242335>
- Lundquist, J. D., Dickerson-Lange, S. E., Lutz, J. A., & Cristea, N. C. (2013). Lower forest density enhances snow retention in regions with warmer winters: A global framework developed from plot-scale observations and modeling: Forests and snow retention. *Water Resources Research*, 49(10), 6356–6370. <https://doi.org/10.1002/wrcr.20504>
- Marks, D., & Dozier, J. (1992). Climate and energy exchange at the snow surface in the alpine region of the Sierra Nevada: 2. Snow cover energy balance. *Water Resources Research*, 28(11), 3043–3054. <https://doi.org/10.1029/92WR01483>
- McGrath, D., Zeller, L., Bonnell, R., Reis, W., Kampf, S., Williams, K., Okal, M., Olsen-Mikutowicz, A., Bump, E., Sears, M., & Rittger, K. (2023). Declines in peak snow water equivalent and elevated snowmelt rates following the 2020 Cameron peak wildfire in northern Colorado. *Geophysical Research Letters*, 50(6), e2022GL101294. <https://doi.org/10.1029/2022GL101294>
- Micheletty, P. D., Kinoshita, A. M., & Hogue, T. S. (2014). Application of MODIS snow cover products: Wildfire impacts on snow and melt in the Sierra Nevada. *Hydrology and Earth System Sciences*, 18(11), 4601–4615. <https://doi.org/10.5194/hess-18-4601-2014>
- Mooser, C. D., Broxton, P. D., Harpold, A., & Robertson, A. (2020). Estimating the effects of Forest structure changes from wildfire on snow water resources under varying meteorological conditions. *Water Resources Research*, 56(11), e2020WR027071. <https://doi.org/10.1029/2020WR027071>
- Moriasi, D. N., Arnold, J. G., Liew, M. W. V., Bingner, R. L., Harmel, R. D., & Veith, T. L. (2007). Model evaluation guidelines for systematic quantification of accuracy in watershed simulations. *Transactions of the ASABE*, 50(3), 885–900. <https://doi.org/10.13031/2013.23153>
- Mote, P. W., Li, S., Lettenmaier, D. P., Xiao, M., & Engel, R. (2018). Dramatic declines in snowpack in the western US. *Npj Climate and Atmospheric Science*, 1(1), 2. <https://doi.org/10.1038/s41612-018-0012-1>
- Musselman, K. N., Molotch, N. P., & Brooks, P. D. (2008). Effects of vegetation on snow accumulation and ablation in a mid-latitude sub-alpine forest. *Hydrological Processes*, 22(15), 2767–2776. <https://doi.org/10.1002/hyp.7050>
- NOAA, C. (2021). “Climate data online (CDO).”. The National Climatic Data Center’s (NCDC) climate data online (CDO) provides free access to NCDC’s archive of historical weather and climate data in addition to station history information. National Climatic Data Center (NCDC).
- R Core Team. (2021). “R: A language and environment for statistical computing.”. R Foundation for Statistical Computing <https://www.R-project.org/>
- Rodman, K. C., Veblen, T. T., Battaglia, M. A., Chambers, M. E., Fornwalt, P. J., Holden, Z. A., Kolb, T. E., Ouzts, J. R., & Rother, M. T. (2020). A changing climate is snuffing out post-fire recovery in montane forests. *Global Ecology and Biogeography*, 29(11), 2039–2051. <https://doi.org/10.1111/geb.13174>
- Saha, S., Moorthi, S., Wu, X., Wang, J., Nadiga, S., Tripp, P., Behringer, D., Hou, Y.-T., Chuang, H., Iredell, M., Ek, M., Meng, J., Yang, R., Mendez, M. P., van den Dool, H., Zhang, Q., Wang, W., Chen, M., & Becker, E. (2011). *NCEP climate forecast system version 2 (CFSv2) 6-hourly products*. Research Data Archive at the National Center for Atmospheric Research, Computational and Information Systems Laboratory. <https://doi.org/10.5065/D61C1TXF>
- Sexstone, G. A., Clow, D. W., Fassnacht, S. R., Liston, G. E., Hiemstra, C. A., Knowles, J. F., & Penn, C. A. (2018). Snow sublimation in mountain environments and its sensitivity to Forest disturbance and climate warming. *Water Resources Research*, 54(2), 1191–1211. <https://doi.org/10.1002/2017WR021172>
- Sicart, J. E., Essery, R. L. H., Pomeroy, J. W., Hardy, J., Link, T., & Marks, D. (2004). A sensitivity study of daytime net radiation during snowmelt to Forest canopy and atmospheric conditions. *Journal of Hydrometeorology*, 5(5), 774–784. [https://doi.org/10.1175/1525-7541\(2004\)005<0774:ASSODN>2.0.CO;2](https://doi.org/10.1175/1525-7541(2004)005<0774:ASSODN>2.0.CO;2)
- Smoot, E. E., & Gleason, K. E. (2021). Forest fires reduce snow-water storage and advance the timing of snowmelt across the Western U.S. *Water*, 13(24), 24. <https://doi.org/10.3390/w13243533>
- Stevens, J. T. (2017). Scale-dependent effects of post-fire canopy cover on snowpack depth in montane coniferous forests. *Ecological Applications*, 27(6), 1888–1900. <https://doi.org/10.1002/eap.1575>
- Stevens-Rumann, C. S., Kemp, K. B., Higuera, P. E., Harvey, B. J., Rother, M. T., Donato, D. C., Morgan, P., & Veblen, T. T. (2018). Evidence for declining forest resilience to wildfires under climate change. *Ecology Letters*, 21(2), 243–252. <https://doi.org/10.1111/ele.12889>
- Stevens-Rumann, C. S., & Morgan, P. (2019). Tree regeneration following wildfires in the western US: A review. *Fire Ecology*, 15(1), 15. <https://doi.org/10.1186/s42408-019-0032-1>
- U.S. Geological Survey National Geospatial Program. (2022). *USGS National Hydrography Dataset Plus High Resolution National Release 1 FileGDB (dataset)*. U.S. Geological Survey. <https://doi.org/10.5066/P9WFOBQI>
- Ueyama, M., Ichii, K., Iwata, H., Euskirchen, E. S., Zona, D., Rocha, A. V., Harazono, Y., Iwama, C., Nakai, T., & Oechel, W. C. (2014). Change in surface energy balance in Alaska due to fire and spring warming, based on upscaling eddy covariance measurements: Change in high-latitude energy balance. *Journal of Geophysical Research: Biogeosciences*, 119(10), 1947–1969. <https://doi.org/10.1002/2014JG002717>
- USDA-NRCS. (2020). “SNOWpack TELEmetry Network (SNOTEL)/Ag Data Commons.”. <https://data.nal.usda.gov/dataset/snowpack-telemetry-network-snotel>
- Vanderhoof, M. K., Hawbaker, T. J., Ku, A., Merriam, K., Berryman, E., & Cattau, M. (2021). Tracking rates of postfire conifer regeneration vs. deciduous vegetation recovery across the western United States. *Ecological Applications*, 31(2), e02237. <https://doi.org/10.1002/eap.2237>
- Varhola, A., Coops, N. C., Weiler, M., & Moore, R. D. (2010). Forest canopy effects on snow accumulation and ablation: An integrative review of empirical results. *Journal of Hydrology*, 392(3–4), 219–233. <https://doi.org/10.1016/j.jhydrol.2010.08.009>
- Venables, W. N., & Ripley, B. D. (2002). *Modern applied statistics with S (fourth)*. Springer. <https://www.stats.ox.ac.uk/pub/MASS4/>
- Viana-Soto, A., García, M., Aguado, I., & Salas, J. (2022). Assessing post-fire forest structure recovery by combining LiDAR data and Landsat time series in Mediterranean pine forests. *International Journal of Applied Earth Observation and Geoinformation*, 108, 102754. <https://doi.org/10.1016/j.jag.2022.102754>
- Viviroli, D., Dürr, H. H., Messerli, B., Meybeck, M., & Weingartner, R. (2007). Mountains of the world, water towers for humanity: Typology, mapping, and global significance. *Water Resources Research*, 43(7), W07447. <https://doi.org/10.1029/2006WR005653>
- Westerling, A. L. (2016). Increasing western US forest wildfire activity: Sensitivity to changes in the timing of spring. *Philosophical Transactions of the Royal Society B: Biological Sciences*, 371(1696), 20150178. <https://doi.org/10.1098/rstb.2015.0178>
- Western Regional Climate Center. (2021). “RAWS USA Climate Archive.”. <https://raws.dri.edu/>
- Wieder, W. R., Kennedy, D., Lehner, F., Musselman, K. N., Rodgers, K. B., Rosenbloom, N., Simpson, I. R., & Yamaguchi, R. (2022). Pervasive alterations to snow-dominated ecosystem functions under climate change. *Proceedings of the National Academy of Sciences*, 119(30), e2202393119. <https://doi.org/10.1073/pnas.2202393119>

- Williams, A. P., Livneh, B., McKinnon, K. A., Hansen, W. D., Mankin, J. S., Cook, B. I., Smerdon, J. E., Varuolo-Clarke, A. M., Bjarke, N. R., Juang, C. S., & Lettenmaier, D. P. (2022). Growing impact of wildfire on western US water supply. *Proceedings of the National Academy of Sciences*, 119(10), e2114069119. <https://doi.org/10.1073/pnas.2114069119>
- Yuan, X., Wood, E. F., Luo, L., & Pan, M. (2011). A first look at climate forecast system version 2 (CFSv2) for hydrological seasonal prediction. *Geophysical Research Letters*, 38(13), L13402. <https://doi.org/10.1029/2011GL047792>
- Zambrano-Bigiarini, M. (2020). "hydroGOF: Goodness-of-fit functions for comparison of simulated and observed hydrological time series (0.4-0) (Computer software)". <https://doi.org/10.5281/zenodo.839854>

SUPPORTING INFORMATION

Additional supporting information can be found online in the Supporting Information section at the end of this article.

How to cite this article: Surunis, A., & Gleason, K. E. (2024). Modelling postfire recovery of snow albedo and forest structure to understand drivers of decades of reduced snow water storage and advanced snowmelt timing. *Hydrological Processes*, 38(7), e15246. <https://doi.org/10.1002/hyp.15246>